High-spin studies of ^{172,173}Os: Complex alignment mechanism

J. C. Wells
Oak Ridge National Laboratory, Oak Ridge, Tennessee 37831
and Tennessee Technological University, Cookeville, Tennessee 38505

N. R. Johnson, C. Baktash, I. Y. Lee, and F. K. McGowan
Oak Ridge National Laboratory, Oak Ridge, Tennessee 37831

M. A. Riley* and A. Virtanen†
Oak Ridge National Laboratory and Joint Institute for Heavy Ion Research, Oak Ridge, Tennessee 37831

J. Dudek
Joint Institute for Heavy Ion Research, Oak Ridge, Tennessee 37831
and Université Louis Pasteur, F-67037, Strasbourg CEDEX, France
(Received 13 January 1989)

High-spin states of ^{172}Os have been investigated by γ-γ coincidence studies. These states were populated by the ^{144}Nd(^{32}S,4n) reaction using 162-MeV ^{32}S ions. Gamma-gamma coincidence measurements were made with a Compton-suppression spectrometer system. The yrast band was observed up through the 30^+ state, and four sidebands were deduced from γ-γ coincidence relationships. A band identified as belonging to ^{173}Os was also observed. Results were interpreted using average nuclear field calculations which incorporated the deformed Woods-Saxon potential with its "universal" parametrization, a cranking approximation, and the Hartree-Fock-Bogoliubov method. The calculations indicate the presence of strongly interacting quasiparticle band crossings for $0.2 < \hbar\omega < 0.3$, in semiquantitative agreement with experiment. Both the quasiparticle band structures and decline of neutron pairing are discussed.

I. INTRODUCTION

Recent developments in nuclear structure have brought a considerable focusing on the problems of shape evolution and shape-coexistence phenomena. Current emphasis is not just on the geometrical shapes, which are relatively easy to think of in terms of various forms of the nuclear surface, but, more importantly, on an understanding of the underlying microscopic forces from the different single-particle configurations, which influence in a dramatic way the changes in nuclear global properties. The nuclei in the light-mass tungsten-osmium region exhibit a richness in both shape-coexistence effects and shape-evolution tendencies and, thus, present excellent opportunities for comprehensive experimental and theoretical investigations. With this in mind, we have carried out a study of ^{172}Os and, as a by-product of the work, have obtained some information on the previously unstudied nucleus, ^{173}Os.

Previous studies[1,2] of ^{172}Os have established the yrast sequence up to $I=24^+$. Durell *et al.*[1] also reported one partially developed sideband with some interband transitions to the ground band, and Wells *et al.*[2] reported some of these same transitions, but gave no level ordering for this sideband. Both Durell *et al.*[1] and Wells *et al.*[2] reported two anomalies in the yrast-sequence moment of inertia below a rotational frequency $\hbar\omega=0.27$ MeV. The first of these anomalies occurs at an unusually low spin, $I=8^+$, and at a rotational frequency $\hbar\omega=0.24$ MeV, and the second occurs at $I=16^+$ and $\hbar\omega=0.27$ MeV. The suggestion[1] that a shape-coexistence picture may be applicable to ^{172}Os with a significant jump in deformation at $I=8^+$ was investigated by Wells *et al.*[2] through self-consistent cranked-shell-model calculations. However, only a smooth increase of $\Delta\beta_2=0.02$ with increasing frequency for the ground configurations was found over a frequency range extending to about 0.25 MeV.

In the earlier work,[2] the possibility that the anomaly at $I=8^+$ arose from an additional band crossing, a situation consistent with the behavior of the dynamical moment of inertia $\mathcal{J}^{(2)}$, was explored. Specifically, we considered the possibility that early alignment of $h_{9/2}$ $[541]\frac{1}{2}$ protons may be a contributor. Although this seemed implausible (since the cranking calculations predicted such alignment to occur at much higher frequency, $\hbar\omega\approx0.45$ MeV), we were able to produce a very good theoretical fit to the discontinuities in the $\mathcal{J}^{(2)}$ plot through a phenomenological three-band-mixing calculation. Recently, Dracoulis *et al.*[3] also carried out three-band-mixing calculations on ^{172}Os, as well as on ^{170}Os, and concluded that the behavior of the total aligned angular momentum could be fit by invoking the presence of "intruder" band heads at 600 and 1200 keV, respectively.

The idea of a "third" band has also been proposed[4] to explain similar anomalies in the yrast sequences of heavier even-even osmium isotopes, where the Fermi level lies among the larger-Ω components of the $i_{13/2}$ neutrons. In this situation, the lowest quasineutron levels, which are not completely aligned below the band crossing, gain alignment in the frequency range of the strongly

interacting-band-crossing; i.e., a "third" configuration mixes in during the band crossing. However, it seems that such an explanation is not likely for ^{172}Os, where the Fermi level lies lower in the neutron shell among the low-$\Omega, i_{13/2}$ components. Indeed, the abrupt increase in the signature splitting for the lowest positive-parity single quasineutron levels in the neighboring odd-N isotopes argues against this explanation for ^{172}Os.

Interestingly, Hsieh *et al.*[5] have recently carried out calculations using an interacting-boson-approximation (IBA)-plus-two-quasiparticle model in which they considered the $i_{13/2}$ neutron and $h_{9/2}$ proton orbitals. They applied these to the even osmium nuclei from mass 172 to 180 and concluded that it was necessary to invoke major contributions from the $h_{9/2}$ protons to explain the behavior in the yrast sequence of ^{172}Os.

Since the earlier work[1,2] had left many interesting and unanswered questions about ^{172}Os, we have made a detailed reinvestigation of this nucleus. Compton-suppressed γ-ray data of good statistical quality have provided new details on the yrast sequence and have enabled us to construct four sidebands. In addition, refined cranking calculations using a deformed Woods-Saxon potential and the Hartree-Fock-Bogoliubov method have led to an improved understanding of this nucleus. These are the topics of the present study to be covered below. We[6–8] have also carried out Doppler-shift recoil-distance lifetime measurements on ^{172}Os, but these will be reported in a separate publication.

II. EXPERIMENTAL METHOD

For these measurements, a 1-mg/cm^2 target of enriched ^{144}Nd and a 162-MeV beam of ^{32}S ions from the HHIRF Tandem Accelerator were used, with the 4n-reaction channel producing ^{172}Os. A series of short measurements taken at bombarding energies of 155, 162, and 171 MeV showed that the yield of the 4n-reaction channel was optimized at a beam energy of 162 MeV. The measurements were made with the Oak Ridge Compton Suppression Spectrometer System, which at that time consisted of 19 Compton-suppressed Ge detectors. This system was incorporated into the spin spectrometer, a 4π array of 72 NaI detectors, by replacing 19 of the NaI units with Compton-suppressed Ge units. In this way, we were able to collect 56 million γ-γ coincidence events while recording the associated total energy and γ-ray multiplicity. However, because the reaction-channel selection was not greatly enhanced by total-energy and multiplicity gating in this experiment, we chose to use all coincidence events to improve the statistical quality of the spectra.

With the thin target used, the reaction products recoiled from the target and decayed in flight, and the γ rays were fully Doppler shifted. However, the γ-ray energies were measured in a separate experiment by using a Pb-backed target which stopped the recoiling nuclei and eliminated the problem of correcting for Doppler shift. The energy calibration was performed with a standard ^{152}Eu source. This source and a ^{182}Ta source were used to obtain the efficiency calibration for the summed spectra from all 19 detectors. Next, the γ-ray spectra from the 19 Ge detectors were gain-matched and a 4096×4096-channel coincidence matrix was generated using coincidences between all possible pairs of detectors. Note that our earlier investigation[2] of ^{172}Os had indicated that there was not a significant amount of low-energy structure in the γ-ray spectrum. Therefore, we made no special effort to optimize the counting efficiency below about 200 keV in the current measurements.

Some of the Ge detectors were located at 24° and 87° (and at their supplements: 156° and 93°) and thus, we were able to extract angular correlation information from the γ-γ coincidence data. We utilized the standard directional-correlation-from-oriented-states (DCO) relationship[9] of the form

$$R=\frac{W(\theta_1=24°,\theta_2=87°)}{W(\theta_1=87°,\theta_2=24°)}\ , \tag{1}$$

where $W(\theta_1,\theta_2)$ is the angular-correlation function and θ_1 and θ_2 are the angles at which two coincident γ rays are observed with respect to the beam direction. The measurements were made by the observation of a γ ray detected at 24° (or 87°) in coincidence with a known stretched-$E2$ reference transition at 87° (or 24°). For fully aligned nuclei, the ratio of these intensities, $I(87°,24°)/I(24°,87°)$ is approximately a factor of 2 larger for stretched-quadrupole than for stretched-dipole transitions. These DCO ratios were normalized so that the mean of the ratios of the expected stretched-$E2$ transitions in the yrast sequence was unity. Transitions with a spin change of two units were assumed to be $E2$.

III. EXPERIMENTAL RESULTS FOR ^{172}Os

Transition energies, relative γ-ray transition intensities, DCO ratios, and proposed spin-parity assignments for ^{172}Os are given in Table I. The level scheme for ^{172}Os, as deduced from the coincidence data, is shown in Fig. 1, where the ^{172}Os γ rays have been grouped into five bands. The levels up to spin 24^+ in the yrast band have been reported[1,2] previously. Ordering of the γ rays in the level scheme is based on the observed coincidence relationships, on intensity arguments, and on energy systematics. A spectrum gated on the sum of transitions deexciting yrast states from 2^+ to 10^+, showing the prominent transitions from all of these bands and the overall quality of the data, is displayed in Fig. 2.

In Fig. 3, a spectrum gated on the γ rays deexciting yrast sequence states from 14^+ to 26^+ reveals the higher-spin members of the yrast sequence up to spin 30^+. The DCO ratios used to establish the spin assignments in the yrast sequence are shown in Fig. 4. As already pointed out, the ratios of the intensities, $I(87°,24°)/I(24°,87°)$ have been normalized so that the mean for expected stretched-$E2$ transitions is unity. Clearly, the 8^+ and higher transitions in this band are of stretched-$E2$ character. It is observed, however, that the $2^+\rightarrow 0^+$, $4^+\rightarrow 2^+$, and $6^+\rightarrow 4^+$ transitions show reduced DCO ratios. This is a general feature of lower-spin transitions and may result from some loss of alignment.

The spectra obtained by gating on 635- and 624-keV γ

TABLE I. Gamma-ray transition energies, relative γ-ray transition intensities, DCO ratios, and spin-parity assignments for ^{172}Os.

E_γ (keV)[a]	Intensity[b]	DCO Ratio[c]	I_i^π	I_f^π
128.0±0.3	2.0±1.0			13(−)
220.3	2.9±0.4		(8−)	(6−)
227.8	82.1±1.5[d]	0.65±0.03	2+	0+
261.2±0.3	1.5±0.3		(10−)	9(−)
322.0	15.0±0.6	0.87±0.11	7(−)	5(−)
350.8±0.2	2.5±0.4		9(−)	10+
353.7	2.7±0.5		(10−)	(8−)
369.4	8.3±0.5		(12−)	(10−)
378.4	100.0±1.3	0.81±0.03	4+	2+
391.2	19.3±0.7	1.09±0.21	11(−)	9(−)
396.2	28.5±0.8	1.01±0.19	9(−)	7(−)
405.0±0.3	2.9±0.6		(6−)	5(−)
428.7	20.8±1.0	0.99±0.13	13(−)	11(−)
439.8±0.3	0.9±0.5		(12−)	12+
448.4	88.9±1.8	0.92±0.03	6+	4+
453.5	12.3±0.9	0.63±0.13	7(−)	8+
470.5	65.8±1.8	1.00±0.03	8+	6+
471.2±0.2	6.4±0.9			
476.1	6.9±0.8			
488.5	24.7±1.1	1.05±0.07	16+	14+
498.9	54.8±1.5	0.98±0.04	10+	8+
508.3	12.4±0.9		(14−)	(12−)
516.9	18.1±1.1	1.17±0.25	15(−)	13(−)
525.4	10.9±0.9			
536.7	35.2±1.3	0.99±0.04	14+	12+
540.6	47.6±1.5	0.98±0.03	12+	10+
555.1	9.3±0.6		(16−)	(14−)
556.3±0.3	4.2±1.0			
564.9±0.2	6.6±0.8			
565.6	18.4±0.8	0.98±0.13	17(−)	15(−)
572.0	7.5±0.6		(18−)	(16−)
586.8	24.0±0.8	1.19±0.10	18+	16+
591.5±0.3	9.0±0.6			
595.6	14.0±0.7	0.89±0.12	19(−)	17(−)
601.7	11.2±0.7	0.53±0.10	5(−)	6+
605.0	5.9±0.6		(20−)	(18−)
611.6±0.3	2.1±1.0		(10−)	9(−)
612.6±0.2	5.4±0.5			
618.1	10.7±0.5		(21−)	19(−)
623.9	9.7±0.5		(16+′)	(14+′)
630.0±0.3	3.5±0.4			
634.9	10.4±0.5		(14+′)	12+
644.4±0.2	3.2±0.4		(23−)	(21−)
647.4	4.3±0.4		(22−)	(20−)
655.1	15.6±0.5	0.95±0.11	20+	18+
664.6±0.3	5.2±0.5			
684.2±0.2	2.5±0.5		(25−)	(23−)
687.4	5.5±0.4		(18+′)	(16+′)
692.3	3.0±0.5		(24−)	(22−)
696.6	9.4±0.5	1.19±0.31	22+	20+
709.1±0.2	2.7±0.4			
723.9±0.3	3.0±0.5		(20+′)	(18+′)
730.3	4.4±0.4		(24+)	22+
741.8±0.3	2.0±0.5		(26−)	(24−)
742.5±0.3	1.7±0.4			
751.0±1.0	3.5±0.5		(22+′)	(20+′)
769.5	2.3±0.4		(26+)	(24+)
792.5±0.3	2.9±0.6		(28−)	(26−)
814.6±0.2	1.4±0.5		(28+)	(26+)
847.5±0.3	1.7±0.5		(30+)	(28+)
924.1±0.2	5.0±0.4	0.74±0.15	7(−)	6+
1006.6±0.3	4.3±0.4		(6−)	6+
1049.8±0.2	8.0±0.5	0.50±0.30	5(−)	4+

[a]Uncertainty in transition energies is 0.1 keV unless otherwise stated.
[b]Relative γ-ray intensities are normalized to the intensity of the $4^+ \rightarrow 2^+$ transition (= 100).
[c]The DCO ratios are defined by Eq. 1 in the text. Ratios are normalized to unity for stretched-$E2$ transitions in the yrast sequence.
[d]Not corrected for coincidence efficiency.

rays confirmed that these and the 687-keV transition are members of the extension (band 1) beyond the backbend of the ground band up to spin 18^+. Although speculative, there is also some evidence for the 20^+ and 22^+ members of this band extension.

The 471-keV γ ray, which appears in the yrast sequence, was established as a doublet since it also occurs in the 1050-, 602-, and 924-keV gates, and from these it was determined that the $8^+ \rightarrow 6^+$ transition in the yrast sequence has an intensity of 65.8 units and the weaker transition, 6.4 units. The less intense member of this doublet was placed in the same sequence with the 476-keV γ ray by observing that, in the 471-keV gate, the ratio of the intensity of the 471-keV γ ray to that of the 476-keV γ ray was 0.51. This was further confirmed by observing that the ratio of the intensity of the 476-keV γ ray to that of the 429-keV γ ray in the 471-keV gate was significantly larger than the same ratio in the 228-keV gate.

Figure 5 shows a spectrum gated on the 429-, 517-, and 596-keV γ rays. This spectrum reveals the γ rays which were assigned to higher-spin members of band 3 and to transitions from another band feeding into the 5491-keV level. The starred peak in this spectrum is an impurity from an unidentified nuclide. The transitions within this band show DCO ratios characteristic of stretched-quadrupole transitions as can be seen in Fig. 6. Further, the 454-, 602-, 924-, and 1050-keV interband transitions appear to be dipole transitions, since their DCO ratios are all significantly less than unity. Based on the features of band 3 and known systematics, we assume that this band has $(\pi,\alpha)=(-,1)$, commonly called the AE band (additional discussion on the nomenclature and characteristics of the bands built on quasiparticle configurations will appear in Sec. V). In addition, we point out that the assignment of states as a continuation of band 3 beyond the 5491-keV level and those as a sideband feeding in at this point presented some difficulty. All five transitions above the 5491-keV level were in coincidence with a gate set at 618 keV. The problem is that these five transitions are quite weak and, thus, the spectra generated by gating on each one individually are not of good statistical quality. They do lead us to conclude, however, that there are two cascades feeding into the 5491-keV level as shown in

Fig. 1. Based on the aligned angular momentum in band 4 (the signature partner of band 3) and on the systematics of $(-,1)$ bands, we assume that the 644- and 684-keV transitions are members of the $(-,1)$ band of ^{172}Os.

Band 2 is established through coincidence relationships seen in the 396-, 476-, and 525-keV gates. A spectrum gated on the 476- and 525-keV transitions, showing all of the transitions in this band, is displayed in Fig. 7. The transitions in the band were ordered by intensity and energy systematics. Based on branching ratios, approximately 30% of the 471-keV peak intensity in Fig. 7 can be assigned to be $8^+ \rightarrow 6^+$ transition in the ground band. In addition, the 565-keV transition is also part of a doublet, the other member being the 566-keV transition in band 3. The data show that the 391- and 476-keV transitions are in coincidence with each other, indicating that there is an 80-keV transition between the 2846-keV level of band 2 and the 2766-keV level of band 3. A γ ray of this energy was not observed in our coincidence spectra, however. If this transition were of $E1$ multipolarity, its γ-ray intensity would be about 0.3 units and if of $M1$ or $E2$ multipolarity, the γ-ray intensity would be only about 0.05 units. In either case, it would be beyond our detection limits in this region of the spectra. The starred peaks in Fig. 7 are from coincidences in one of the unidentified bands (from another nucleus) having transitions of the same energy as those in our gates.

Members of band 4 are shown in Fig. 8, a spectrum in coincidence with the 369-, 508-, 555-, 572-, 605-, 647-, and 692-keV transitions. These γ rays all show strong coincidence relationships with the 448-, 378-, and 228-keV transitions in the yrast sequence, and weaker coincidence relationships with the 396- and 322-keV transitions in the odd-spin band.

From the coincidence data, we find that a 998.8-keV γ ray feeds into the 10^+ state, implying a level at 3023 keV. The data also indicate that 889.6- and 828.9-keV transitions probably feed the 8^+ state and originate from levels

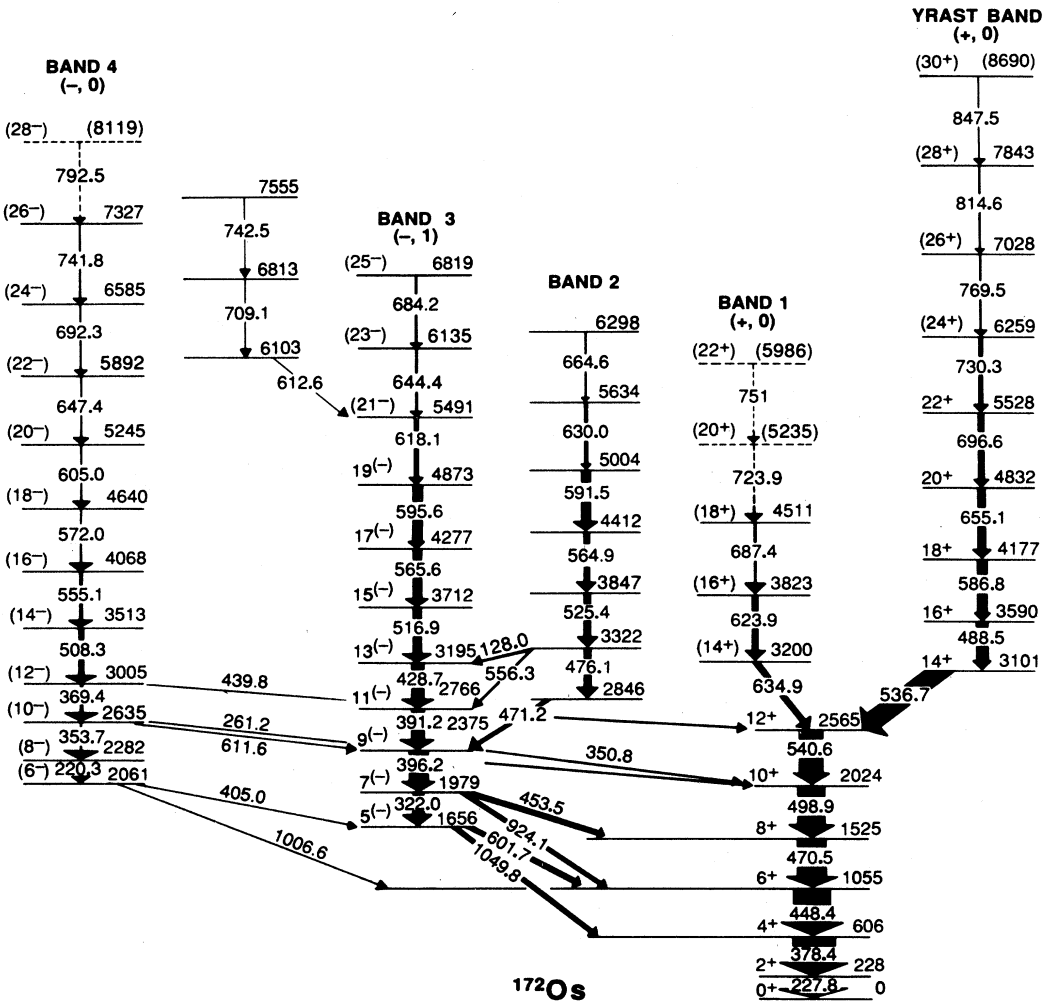

FIG. 1. The level scheme of ^{172}Os. Energies are in keV. Relative transition intensities are indicated by the widths of the arrows. Parentheses and dashes indicate tentative assignments.

at 2415 keV and 2354 keV, respectively. However, because of their questionable nature, we choose not to show these three levels in Fig. 1.

IV. EXPERIMENTAL RESULTS FOR ^{173}Os

We have also identified γ rays belonging to other reaction channels besides the $4n$ channel which leads to ^{172}Os. In addition to γ rays from ^{169}W and ^{170}W, we observe five other distinct bands which, based on x-ray energies, are probably Re and odd-mass Os isotopes.

We have identified one of these bands as being that of ^{173}Os. The level scheme is shown in Fig. 9, and the energies and intensities are given in Table II. A spectrum gated on the 232-keV γ ray is shown in Fig. 10. The identification of $Z=76$ was based on x rays in coincidence with members of this band. The identification of $A=173$ was made by means of excitation-function results.

Bombarding energies of 155, 162, and 171 MeV were used for the ^{32}S ions. The intensities of the 232- and 484-keV transitions for these three bombarding energies are shown in Fig. 11. Also shown are the intensities of the 228- and 378-keV transitions in ^{172}Os. We see that both γ rays from ^{172}Os, which is formed by a four-particle evaporation process, have more or less equal intensities at bombarding energies of 155 and 162 MeV, and begin to fall off at 171 MeV. Therefore, the 232- and 484-keV γ

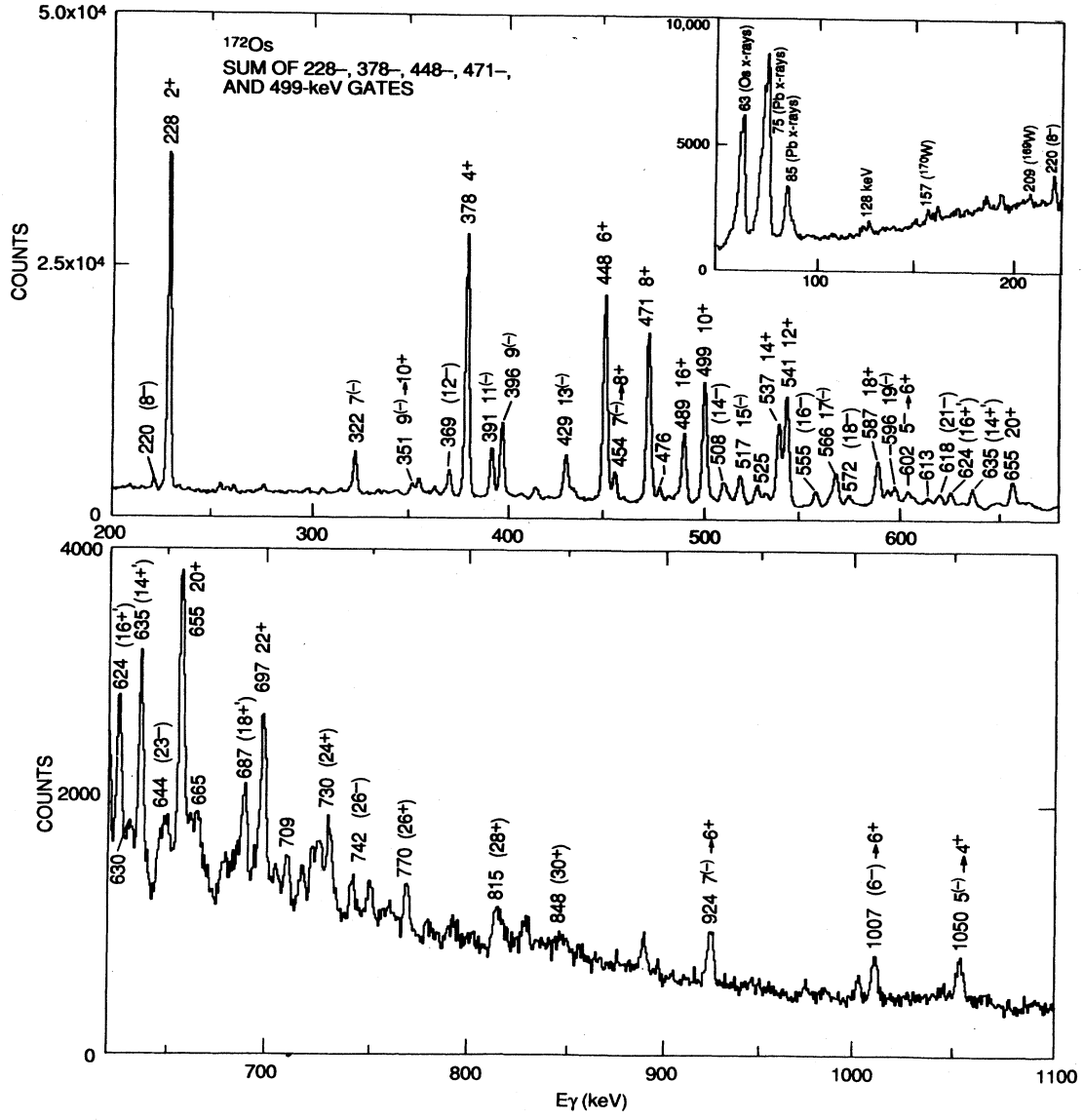

FIG. 2. Spectrum of γ rays in coincidence with 228-, 378-, 448-, 471-, and 499-keV γ rays from ^{172}Os showing transitions from all five bands and overall quality of the data. Gamma rays from ^{172}Os are labeled with energy in keV and initial spin and parity.

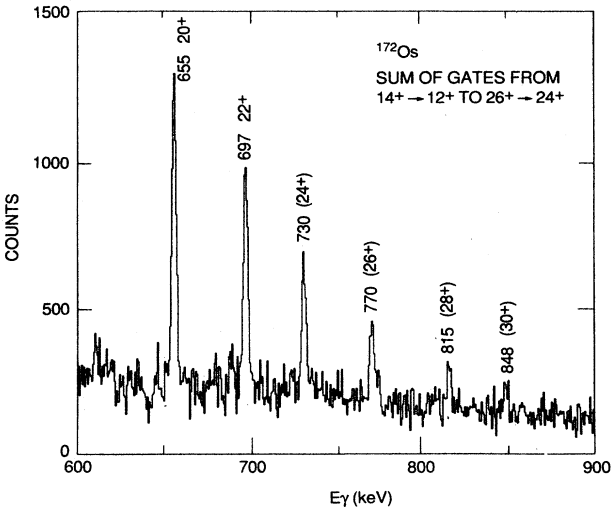

FIG. 3. Spectrum of γ rays in coincidence with γ rays deexciting yrast states between 14^+ and 26^+ showing the high-spin transitions in the yrast band. Gamma rays are labeled with energy in keV and initial spin and parity.

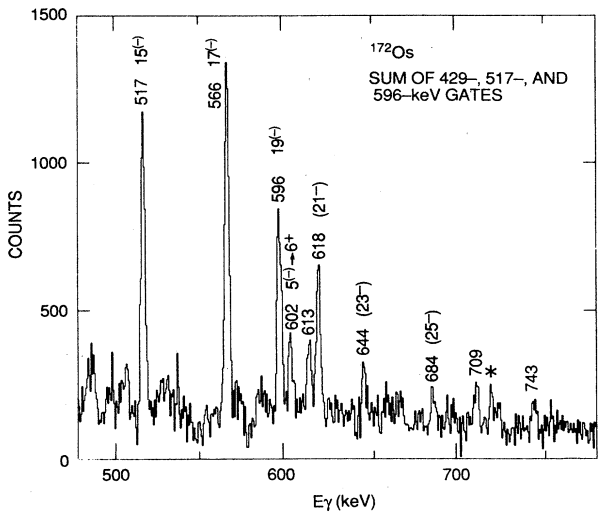

FIG. 5. Spectrum of γ rays in coincidence with the 429-, 517-, and 596-keV γ rays showing high-spin transitions in the odd-spin negative-parity band (band 3) and those transitions feeding into the (21^-) level of band 3. Gamma rays are labeled with energy in keV and initial spin and parity. The peak labeled with (*) is a contaminant from an unidentified nucleus.

rays, whose intensities are already falling off sharply between 155 and 162 MeV, are most likely from a nuclide formed by a three-particle evaporation process. Calculations made with the fusion-evaporation code Julian-PACE[10] are in agreement with these observations and conclusions. We suggest tentative spin and parity values based on the assumption that this is a rotational band with stretched-$E2$ transitions, and that the band-head spin and parity are $\frac{13}{2}^+$, expected from the systematics of odd-neutron nuclei in this region (i.e., the $i_{13/2}$ neutron orbital is near the Fermi surface in this mass region). Since we are probably dealing with the low-Ω projections in the $i_{13/2}$ shell, however, a spin of $\frac{13}{2}$ could not represent the ground state of ^{173}Os. By the same token, the level energies shown here are only relative values.

In addition to the one ^{173}Os band shown in Fig. 9, we also found two other bands which we are reasonably sure belong to this nucleus. However, since the intensities in these two bands are somewhat less and since we were unable to definitely establish any connecting transitions between the three bands, we have chosen to show only the single band in Fig. 9.

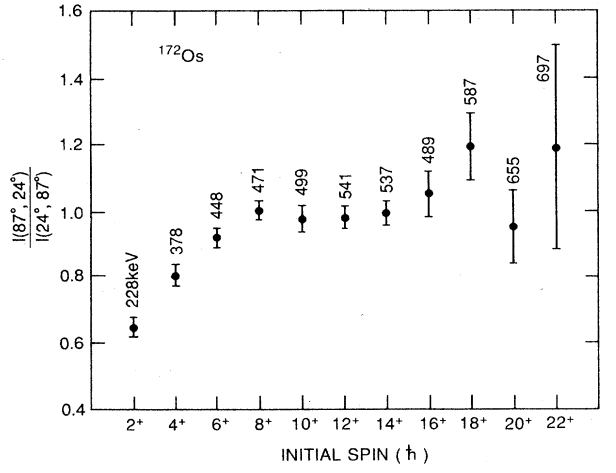

FIG. 4. DCO ratios for members of the yrast sequence in ^{172}Os. The ratios for stretched-$E2$ transitions are normalized to unity.

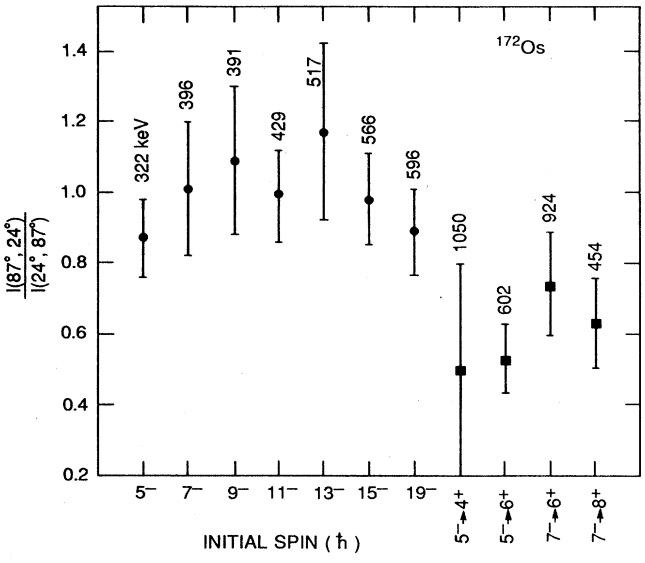

FIG. 6. DCO ratios for members of band 3 and for the interband transitions connecting this band with the ground-state band. The ratios for stretched-$E2$ transitions are normalized to unity.

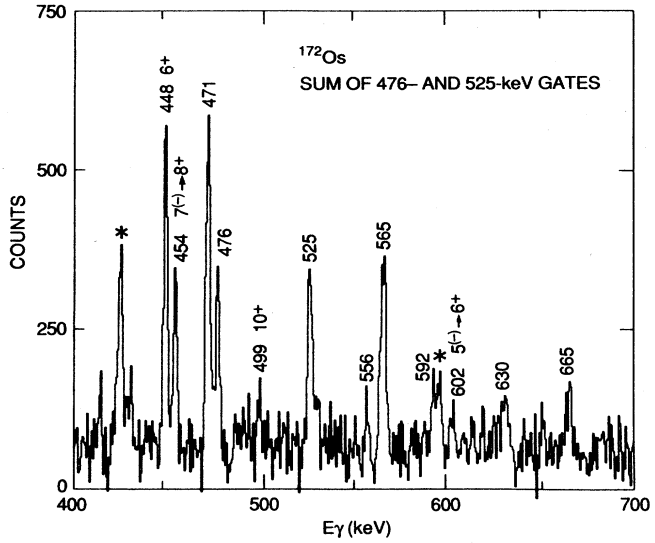

FIG. 7. Spectrum of γ rays in coincidence with the 476- and 525-keV γ rays showing high-spin transitions of band 2. Gamma rays are labeled with energy in keV and initial spin and parity. Peaks labeled with (*) are contaminants from unidentified nuclei.

V. EXPERIMENTAL BAND-CROSSING FREQUENCIES AND ALIGNMENTS IN ^{172}Os AND ^{173}Os

The experimental aligned angular momenta for the five bands in ^{172}Os are shown in Fig. 12(a), and the experimental Routhians are shown in Fig. 12(b). The alignment plot for ^{173}Os is shown in Fig. 13. These plots are labeled by their signature quantum numbers (π,α). The reference subtracted in extracting the experimental quantities was of the form $R_{\text{ref}}=\mathcal{I}_0\omega+\mathcal{I}_1\omega^3$, where the parameters $\mathcal{I}_0=15\hbar^2$ MeV^{-1} and $\mathcal{I}_1=90\hbar^4$ MeV^{-3} were adopted in the present work. These parameters are representative of the optimum values for several nuclei in this region. As seen in Figs. 12 and 13, they produce an approximately constant value of the rotation alignment (i_x relatively flat) at low-rotational frequencies.

The Routhians in Fig. 12(b) are plots of the excitation energies of the excited quasiparticles in the rotating frame, with band crossings appearing as changes in the slope. The convention for labeling the quasiparticles is given in Table III. Note that the A, B, C, and D designations are the lowest-lying quasineutron orbitals from the $i_{13/2}$ shell and the E, F designations are the two lowest-lying quasineutron orbitals from the $h_{9/2}$ shell.

At low frequency, the yrast band is the zero-quasiparticle vacuum configuration. From the composite structure of the yrast line in the frequency range of $\hbar\omega=0.22$–0.28 MeV, one may conclude that there are probably strong interactions between crossing levels and that they involve multiquasiparticle configurations. A discussion of the alignment processes occurring in the yrast sequence through this frequency range will be presented in Sec. VI. Note that at a crossing frequency of 0.26 MeV we do see an increase in alignment of about 10.5 $\hbar$ units. This is considerably more alignment than

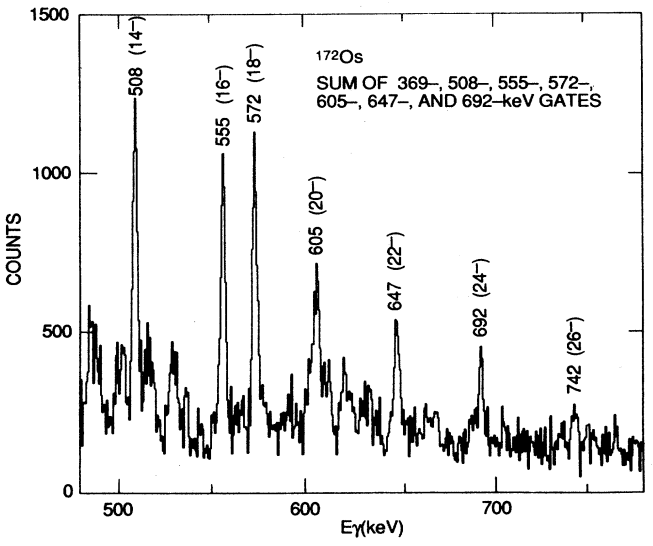

FIG. 8. Spectrum of γ rays in coincidence with the 369-, 508-, 555-, 572-, 605-, 647-, and 692-keV γ rays showing high-spin transitions of band 4. Gamma rays are labeled with energy in keV and initial spin and parity.

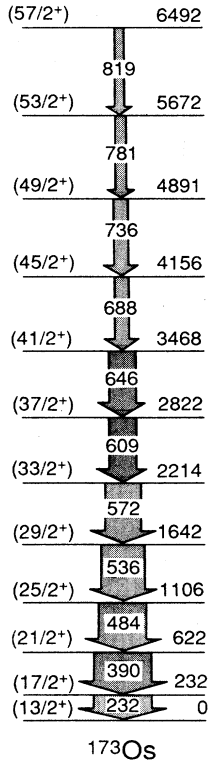

FIG. 9. The level scheme of ^{173}Os. Relative energies are in keV. Relative transition intensities are indicated by the widths of the arrows. The spin assignments are based on the assumption of $I=\frac{13}{2}^+$ for the band head.

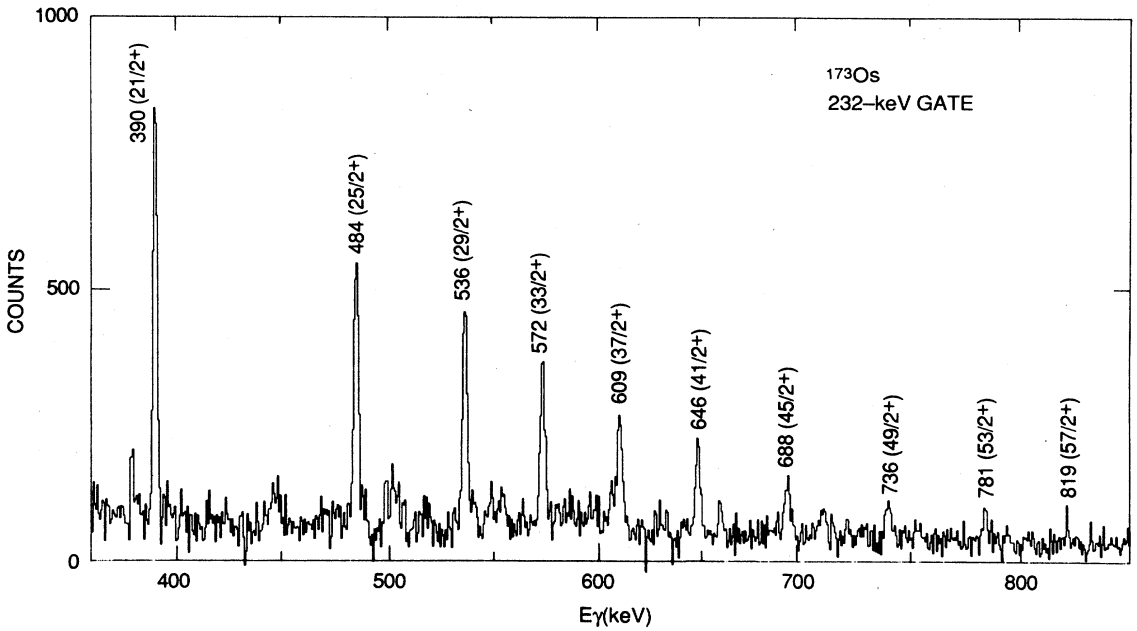

FIG. 10. Spectrum of γ rays in coincidence with the 232-keV γ ray from ^{173}Os. Gamma rays are labeled with energy in keV and initial spin and parity, based on the assumption that the band head spin is $\frac{13}{2}^+$.

we extract from the experimental data for the *AB* crossing in the other isotones of ^{172}Os (see Refs. 11–13).

Based on our experimental data and systematics, we conclude that the low-frequency members of the negative-parity bands are probably two-quasineutron configurations, with the $\alpha=1$ band (band 3) having the *AE* configuration and the $\alpha=0$ band (band 4) having the *AF* configuration. One can see the signature splitting between the *AE* and *AF* configurations in Fig. 12(b). At $\hbar\omega=0.28$ MeV, both of these bands may be crossed by a four-quasineutron configuration in which the *BC* quasineutrons have aligned, giving the $\alpha=1$ band the *AEBC* configuration and the $\alpha=0$ band the *AFBC* configuration. In each case, about $7\hbar$ of alignment gain is produced by the *BC* crossing, and this value agrees closely with that from the *BC* crossing of the *AE* configuration in ^{170}Os (see Ref. 3).

Our data on band 2 were not of sufficient quality to provide spin assignments. However, from the observed

TABLE II. Transition energies, relative γ-ray transition intensities, and spin-parity values for γ rays from ^{173}Os.

E_γ(keV)[a]	Intensity[b]	$I_i^{\pi c}$	$I_f^{\pi c}$
232.4		$(\frac{17}{2}^+)$	$(\frac{13}{2}^+)$
389.5	100±8	$(\frac{21}{2}^+)$	$(\frac{17}{2}^+)$
484.1	88±8	$(\frac{25}{2}^+)$	$(\frac{21}{2}^+)$
535.5	79±8	$(\frac{29}{2}^+)$	$(\frac{25}{2}^+)$
572.2	59±6	$(\frac{33}{2}^+)$	$(\frac{29}{2}^+)$
608.6	50±6	$(\frac{37}{2}^+)$	$(\frac{33}{2}^+)$
645.7	45±5	$(\frac{41}{2}^+)$	$(\frac{37}{2}^+)$
687.7±0.2	32±5	$(\frac{45}{2}^+)$	$(\frac{41}{2}^+)$
735.5±0.2	22±5	$(\frac{49}{2}^+)$	$(\frac{45}{2}^+)$
781.0±0.2	19±4	$(\frac{53}{2}^+)$	$(\frac{49}{2}^+)$
819.4±0.3	11±4	$(\frac{57}{2}^+)$	$(\frac{53}{2}^+)$

[a]Uncertainty in transition energies is 0.1 keV unless otherwise indicated.

[b]Relative γ-ray intensities are normalized to the intensity of the 389.5-keV transition (=100).

[c]Based on the assumption that the band-head spin and parity are $\frac{13}{2}^+$.

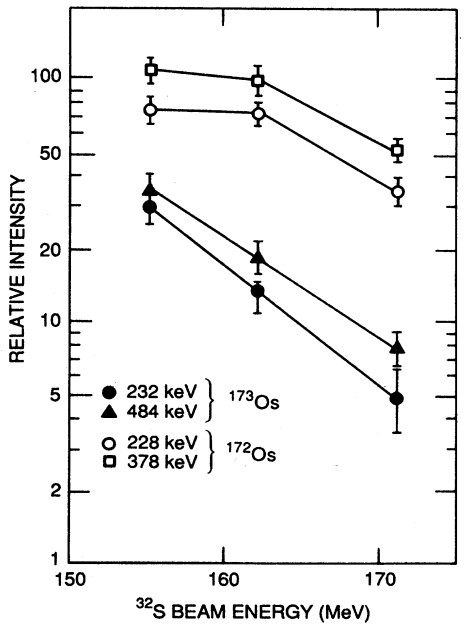

FIG. 11. Excitation function for γ rays from ^{173}Os ($3n$ channel) and ^{172}Os ($4n$ channel).

TABLE III. Convention for labeling the quasiparticles.

Quasiparticle	$(\pi,\alpha)_n$	Label
Quasineutrons	$(+,+\frac{1}{2})_1$	A
	$(+,-\frac{1}{2})_1$	B
	$(+,+\frac{1}{2})_2$	C
	$(+,-\frac{1}{2})_2$	D
	$(-,+\frac{1}{2})_1$	E
	$(-,-\frac{1}{2})_1$	F
Quasiprotons	$(-,-\frac{1}{2})_1$	A_p
	$(-,+\frac{1}{2})_1$	B_p

decay pattern of this band and the known systematics, it seems likely that it is the continuation of the $(-,1)$ octupole band above the point at which it is crossed by the AE band. The decay pattern is consistent with the assumption that the 2846-keV level has spin 11^-. Whereas

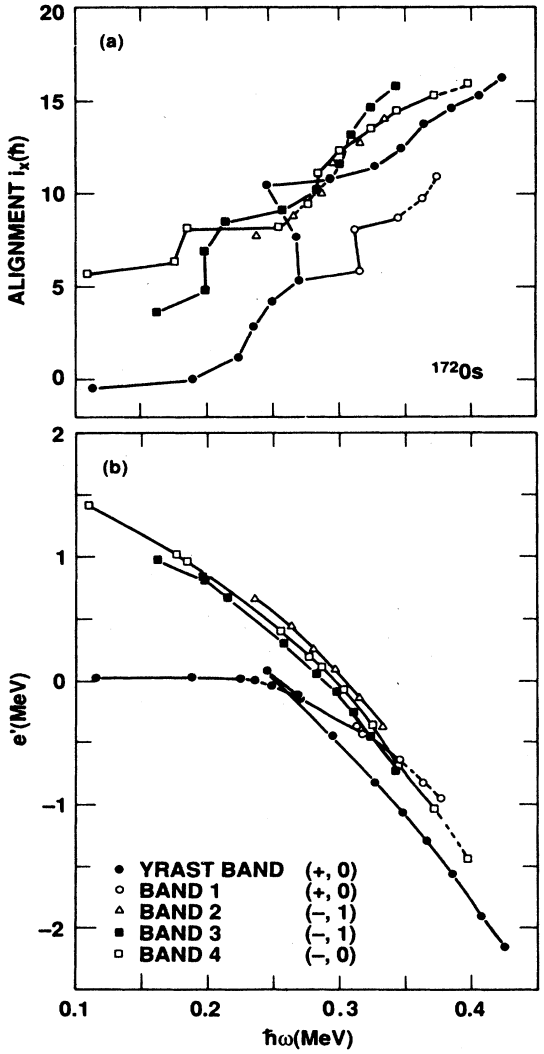

FIG. 12. (a) Aligned angular momentum (i_x), and (b) Routhians for bands in ^{172}Os. All values are deduced from our experimental data.

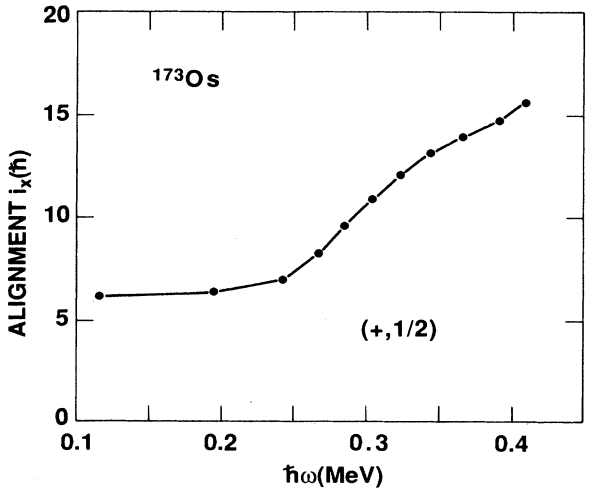

FIG. 13. Aligned angular momentum (i_x) for the band in ^{173}Os as deduced from our experimental data.

K values of 0 were assigned to all of the other bands, we assume that band 2 has $K=2$ for the plots in Fig. 12. The full alignment gain from this crossing cannot be assessed, but it appears to be greater than $5\hbar$.

In Fig. 13 we show the aligned angular momentum as a function of rotational frequency for ^{173}Os, where the reference parameters were the same as those used for ^{172}Os. It is interesting that a comparison of the total angular momentum as a function of frequency for ^{173}Os with that for the $(\pi,\alpha)=(+,\frac{1}{2})$ bands in its neighboring odd-mass isotones shows a somewhat larger value at high spin in ^{173}Os. We speculate that this may result from alignment contributions from protons in the latter case.

VI. THEORETICAL RESULTS

The high-spin behavior of the discussed osmium nuclei is expected to depend on shape evolution and possibly shape coexistence effects. For this reason, the first step in our theoretical analysis involved calculations of the total-energy surfaces of ^{172}Os for the four assigned parity-signature combinations as a function of spin (see Fig. 1). These have been performed by using the generalized Strutinsky approach with the deformed Woods-Saxon potential. We used the so-called "universal" parametrization of this potential which, on the average, performs very well in the description of high-spin phenomena. For the details and an overview of this type of approach, including the treatment of pairing and rotation, the reader is referred to Refs. 14–18 where the method is discussed rather extensively.

A. Shape coexistence and evolution

The richness of the shape phenomena in this mass region is illustrated in Figs. 14(a) and (b) where we show some of the total-energy surfaces for ^{172}Os. Figure 14(a) represents the total-energy surfaces for selected spin values having total parity $\pi=+1$ and signature exponent $\alpha=0$. This figure reveals that there are nine pronounced

shape configurations predicted in ^{172}Os, ranging from moderately deformed ($\beta_2 \simeq 0.2$) to the hyperdeformed[16] ($\beta_2 \simeq 1.0$) minima. Included in these are: two triaxial superdeformed minima with $\gamma \simeq \pm 20°$ and $\beta_2 \simeq 0.5$; yet another pair of superdeformed/hyperdeformed configurations with similar triaxialities at $\beta_2 \simeq 0.8$; and finally, two axially symmetric hyperdeformed minima with well-formed separation potential barriers at $\beta_2 \simeq 1.0$ and $\beta_2 \simeq 1.2$.

Here we limit our discussion only to the moderately deformed configurations, with β_2 varying between $\simeq 0.18$ and 0.22, which are represented with the blue colors in the maps for spins $I^\pi = 6^+, \ldots, 40^+$ in Fig. 14(a). The shape evolution related to these minima has interesting consequences for the comparison of theory and experiment, as discussed below. The most important shape change in the moderate-deformation regime corresponds to the switch from $\gamma \simeq -16°$ at spins below the backbending limit to increased γ values (triaxiality decreased down to $\gamma \simeq -6°$) at spins above the backbending ($I \simeq 18\hbar$ and higher); the details are covered below in the discussion surrounding Fig. 22. This change is accompanied by a slight shrinking of the nucleus and, according to the calculations, is enforced by increasing alignment.

For comparison and for illustration of the typical configuration dependence of the discussed shape properties, the negative-parity landscapes are shown in Fig. 14(b) for spins $I^\pi = 6^-$, 12^-, 18^-, 24^-, 30^-, and 40^-. Two properties deserve noticing. First, the negative-parity configurations with minima at $\beta_2 \simeq 0.2$ do not undergo the shape change discussed above in the context of the positive parity states (the minima of the $\pi = -1$ states remain at $\gamma \simeq -16°$ to $-20°$). Second, the multiminima of the total-energy landscape are in some instances even more pronounced (some separating barriers even more elevated) than found in the positive-parity case.

B. The microscopic origin of the shape and alignment effects in ^{172}Os observed in experiment

Having determined the potential energy surfaces (and their associated deformation parameter values) for ^{172}Os, we next proceeded to examine the microscopic effects giving rise to our experiment observations. For this, Hartree-Fock-Bogoliubov Cranking (HFBC) calculations were carried out with a deformed Woods-Saxon potential and both the related particle-number projection technique and the effects of pairing were incorporated. Some of the specific questions we wished to answer are: (1) What are the quasineutron band crossings that give rise to the complex structure in the moment of the inertia? (2) What role do the protons play below rotational frequencies of $\hbar\omega \approx 0.35$ MeV? (3) What are the interaction strengths in these band crossings? (4) How much is the pairing diminished at these rotational frequencies and how does it affect the properties of ^{172}Os?

The single-particle neutron levels were calculated as a function of the quadrupole deformation (β_2) and these are shown in Fig. 15(a). The calculated single-particle proton levels are shown in Fig. 15(b). These figures indicate that the structure of the total wave functions of the yrast and low-lying states in ^{172}Os is determined by two characteristic factors. First, with the neutron Fermi level λ_ν positioned in between the highly alignable orbitals labeled $i_{13/2}$, $K = \frac{3}{2}$ and $i_{13/2}$, and $K = \frac{5}{2}$, there is a tendency for a strong interplay effect stimulated by the pairing forces (via the pairing-occupation factors) of at least three $\nu i_{13/2}$-related configurations. (Note that independent analyses in terms of the three-band mixing approximation can be found in Refs. 2 and 3.) Second, particularly well-pronounced proton-deformed shell closures appear at $Z = 74$, 76, and 78. This chain gives rise to the noticeably lowered single-particle level density and tends to stabilize the deformation in Os ($Z = 76$) at $\beta_2 \simeq 0.18$.

It is instructive to illustrate the influence of rotation on the shell effects and alignment effects in the case where pairing correlations are present and in that where they are absent. We begin with the neutron single-particle Routhians (no-pairing case) plotted as a function of rotational frequency [Fig. 16(a)]. The shapes of these orbitals ($de/d\omega = -j_x$) are directly related to their alignment contributions ($+j_x$). Various members of the $\nu i_{13/2}$ orbital are labeled and shown by dark solid lines. In the vicinity of the Fermi surface of ^{172}Os, the dominating role of the $i_{13/2}$ orbitals in the alignment process is evident when they are compared with the natural (here negative) parity orbitals, which show little curvature with increasing rotational frequency. The tendency for the strong Coriolis mixing among several consecutive $\nu i_{13/2}$ orbitals can be inferred from the strong repulsion among the Routhians. The strong interaction (mixing) between the consecutive members of the intruder orbital is easy to see at the "crossing frequencies" which correspond roughly to $\hbar\omega_c \simeq 0.07$ MeV ($K = \frac{3}{2}$ with $K = \frac{5}{2}$ orbital crossing), $\hbar\omega_c \simeq 0.22$ MeV ($K = \frac{5}{2}$ with $K = \frac{7}{2}$ orbital crossing), $\hbar\omega_c \simeq 0.35$ MeV ($K = \frac{7}{2}$ with $K = \frac{9}{2}$ orbital crossing), etc.

Illustration of the effect of the pairing coupling scheme is given in Fig. 17(a) where we show the Routhians of the $i_{13/2}$ quasineutrons with K quantum numbers of $\frac{5}{2}$, $\frac{3}{2}$, and $\frac{1}{2}$. A most striking feature of these Routhians is the strongly repulsive interaction between these low-Ω orbitals and the narrow frequency range over which this takes place. As noted in Fig. 17(a), the AB (see Table II for notation) crossing occurs first at $\hbar\omega_c \simeq 0.25$ MeV, followed very closely by the BC and AD crossings at $\hbar\omega_c \simeq 0.26$ MeV. We point out that the symbols used here have only an asymptotic meaning: the K-quantum number becomes exact in the $\omega \to 0$ limit, while the shell-model notations (e.g., $\nu i_{13/2}$ or $\pi h_{9/2}$ symbols) acquire an exact meaning in the limit where the deformation goes to zero. Moreover, in the triaxially deformed nuclei the K-quantum number loses validity, even for nonrotating nuclei ($\omega = 0$). Since the triaxialities involved in the following analysis are relatively moderate and since, as we deduced, the overall character of the quasiparticle diagram is not strongly influenced by replacing the moderately small γ values by $\gamma = 0°$, we use for the qualitative illustration purposes the $\gamma = 0°$ plots. In the quantitative analysis, however, the $\gamma \neq 0$ configurations are explicitly used.

While a unique cranking-model interpretation of strongly interacting bands may sometimes be

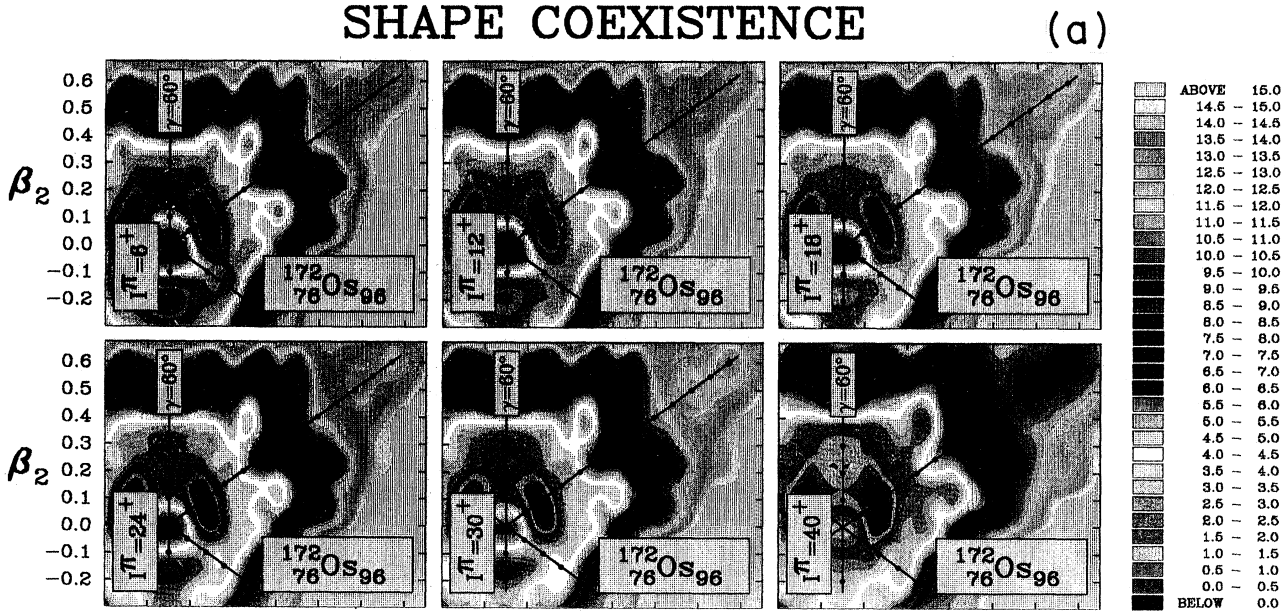

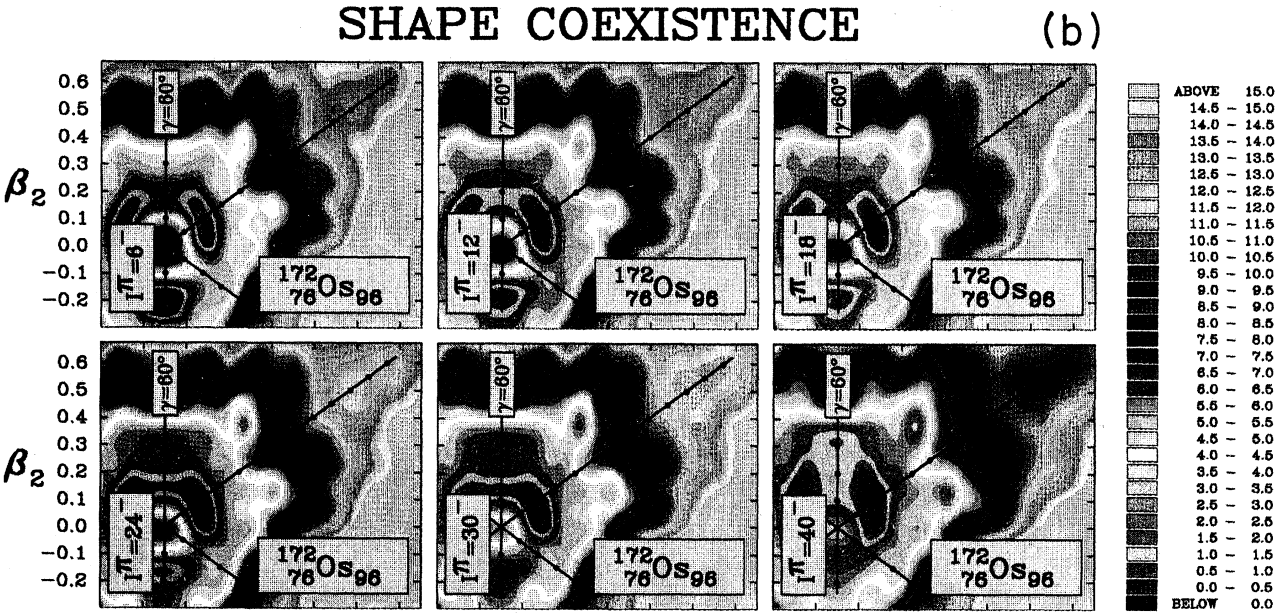

FIG. 14. (a) Total-energy surfaces for positive-parity configurations of ^{172}Os calculated with the extended Strutinsky method (see text). The spin-parity values are given explicitly. The coordinate system is that of the standard (β,γ)-plane with the following convention: vertical axis ($\gamma=60°$) corresponds to increasing oblate shape deformations with the symmetry axis parellel to the cranking axis (noncollective rotation); the $\gamma=0°$ axis (near diagonal) corresponds to increasing elongation where the symmetry axis is perpendicular to the rotation axis (collective rotation); the $\gamma=-60°$ corresponds to the family of oblate shapes identical to those on the $\gamma=+60°$ axis, except that now the symmetry axis is again perpendicular to the rotation axis; finally, the $\gamma=-120°$ axis corresponds to noncollective rotation of the prolate nucleus with the symmetry axis parallel to the spin axis. (b) Similar to that in (a), but for a number of negative-parity configurations.

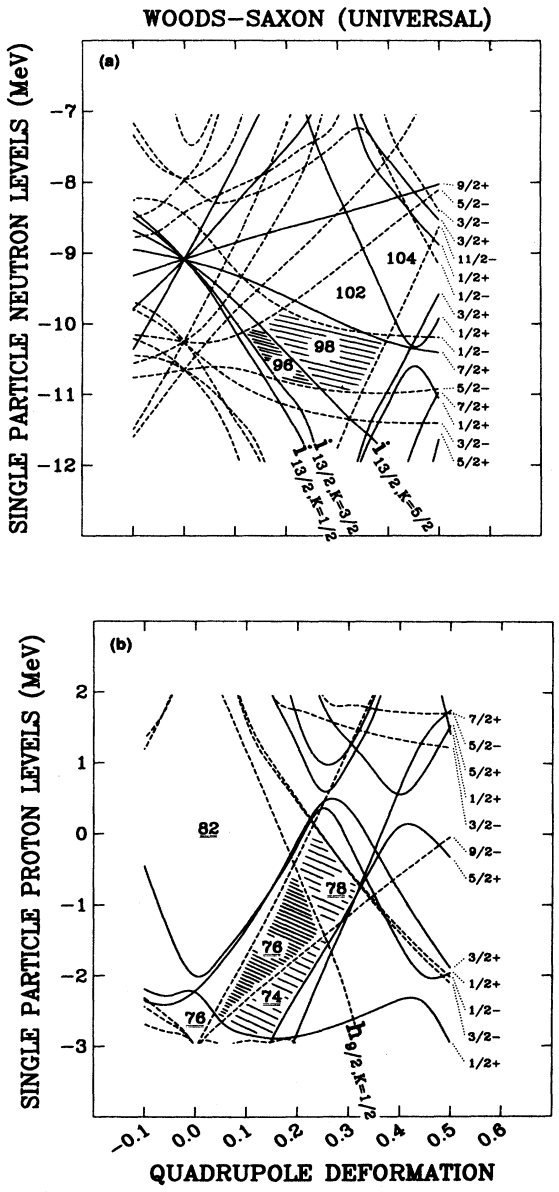

FIG. 15. (a) Calculated single-particle neutron spectrum illustrating the orbitals in the vicinity of $N=96$ (the neutron number of ^{172}Os). The relevant low level-density areas are shaded. Labels on the right-hand side of the figure indicate K^{π}, where K denotes projection of the single-particle angular momentum on the nuclear symmetry axis. The positions of the three lowest (and most important for the alignment properties in ^{172}Os) intruder $i_{13/2}$ orbitals are marked explicitly. The influence of these orbitals on the alignment process in ^{172}Os is illustrated in Figs. 16(a) and 17(a). (b) Calculated single-particle proton spectrum plotted as a function of the quadrupole deformation displaying pronounced deformed shell effects in the vicinity of proton number 76 ($Z=76$ corresponds to osmium). As in (a), the relevant low level-density areas are shaded and the labels on the right-hand side of the figure give the K^{π} quantum numbers. The strongly down-sloping orbital $h_{9/2}, K=\frac{1}{2}$ is labeled explicitly; its importance for the alignment process is evident in Figs. 16(b) and 17(b).

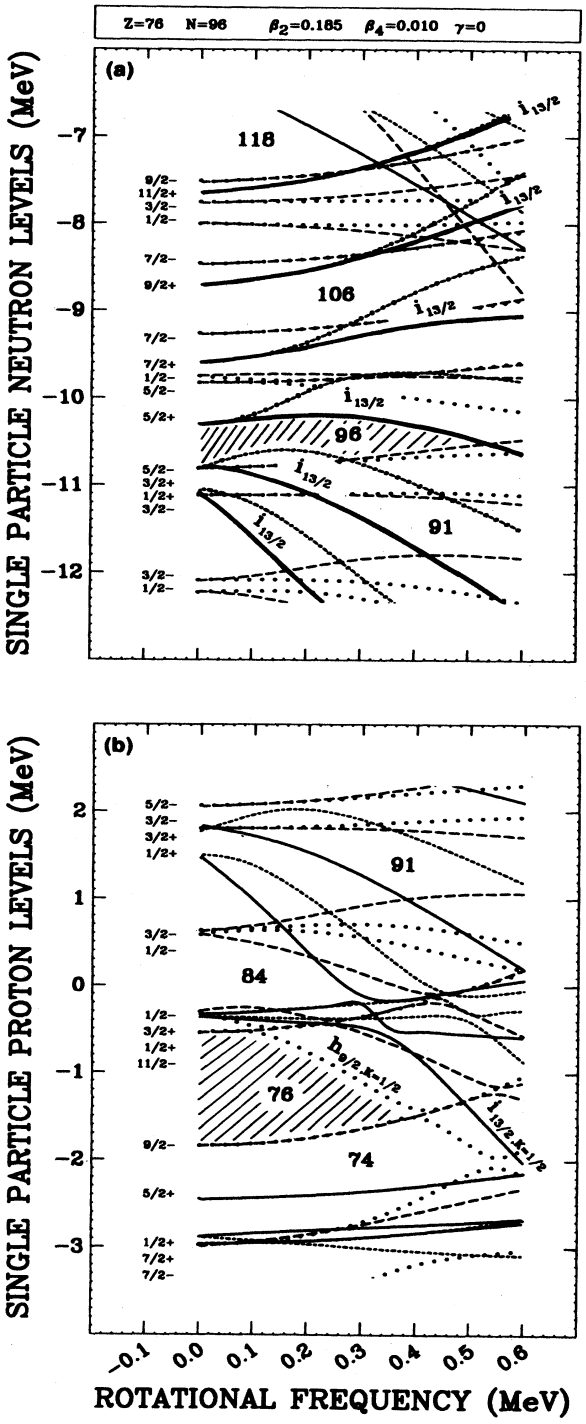

FIG. 16. (a) Neutron single-particle Routhians as a function of the rotational frequency. The deformation parameters used in the calculation are given at the top of the figure. The alignment properties of, in particular, $\nu i_{13/2}$ orbitals (which are shown darkened) deserve noticing. The signature-split orbitals are marked with the conventional symbol of $i_{13/2}$. (b) Similar to that in (a), but for the protons. The two orbitals predicted to play a dominant role at rotational frequencies $\hbar\omega > 0.5$ MeV are labeled $h_{9/2}$, $K=\frac{1}{2}$ and $i_{13/2}$, $K=\frac{1}{2}$.

ambiguous—especially in the cases of shape coexistence and shape changes—the negative-parity bands can relatively safely be attributed to the AE and AF configurations, as illustrated in Fig. 18, where we show the calculated low-lying, negative-parity quasiparticle orbitals for ^{172}Os [see bands denoted $(\pi,\alpha)=(-,1)$ and $(-,0)$ in Fig. 1]. This can be supported further by the very small signature splitting predicted by theory for these two bands, especially in the $\hbar\omega \simeq 0.20$ MeV frequency range. Note the increase in signature splitting above this frequency, both in theory and experiment (Figs. 1, 12, and 18).

For completeness of this discussion, we also present the proton alignment properties. Analogous to Figs. 16(a) and 17(a), the single-particle proton levels are shown in Figs. 16(b) and 17(b). According to the calculations with the "universal" parametrization of the Woods-Saxon potential, the proton orbital most active in the alignment process has the quantum labels $h_{9/2}$, $K=\frac{1}{2}$ and crosses the Fermi level for $Z=76$ at $\hbar\omega \simeq 0.4$ MeV in the zero-pairing Routhians illustrated in Fig. 16(b). It arrives there after a number of crossings with the other negative-parity levels visible in the figure. Inclusion of pairing for the proton system gives rise to the quasiparticle spectrum illustrated in Fig. 17(b). Based on this evidence, we must conclude that it is unlikely that the $h_{9/2}$ quasiprotons play a significant role in the properties of the yrast sequence below $I \simeq 20$.

C. Decline in neutron and proton pairing

It is an inherent part of the pairing self-consistent calculations to produce the prediction of the average pairing behavior as a function of rotational frequency (and the configuration changes induced by rotation). According to the results in Figs. 17(a) and (b), the neutron pairing correlations are strongly diminished over the frequency range $\hbar\omega=0.2-0.3$ MeV. This, according to the Hartree-Fock-Bogoliubov approach, is induced by increasing alignment of the consecutive configurations originating from $\nu i_{13/2}$, $K=\frac{5}{2},\frac{7}{2},\frac{9}{2}$ orbitals. The corresponding effect in the proton phase is predicted to occur at much higher frequencies ($\hbar\omega_c \simeq 0.41$ MeV) as the result of the $h_{9/2}$, $K=\frac{1}{2}$ orbital alignment, followed at $\hbar\omega \simeq 0.55$ MeV by the $\pi i_{13/2}$, $K=\frac{1}{2}$ alignment.

The illustration of the pairing changes due to rotation is given in the bottom parts of Figs. 17(a) and 17(b) in terms of the so-called static pairing gaps Δ_ν, Δ_π. However, at high rotational frequencies, the usually applied HFBC approximation breaks down, and the only self-consistent solutions of the HFBC equations are trivial ($\Delta=0$). The alignment properties can still be well imitated in the high-ω regime if one of the HFBC equations, usually called the gap equation, is dropped (see Ref. 16). Then the Fermi level is found by using an iterative procedure. This is done by solving only the so-called particle number equation at a constant Δ value, typically of the order of 300–500 keV. For this reason, in the results of Figs. 17(a) and 17(b), the high-ω limit corresponds to fixed Δ values. Thus, in the corresponding regime, the quasiparticle diagrams may still be attributed a physical

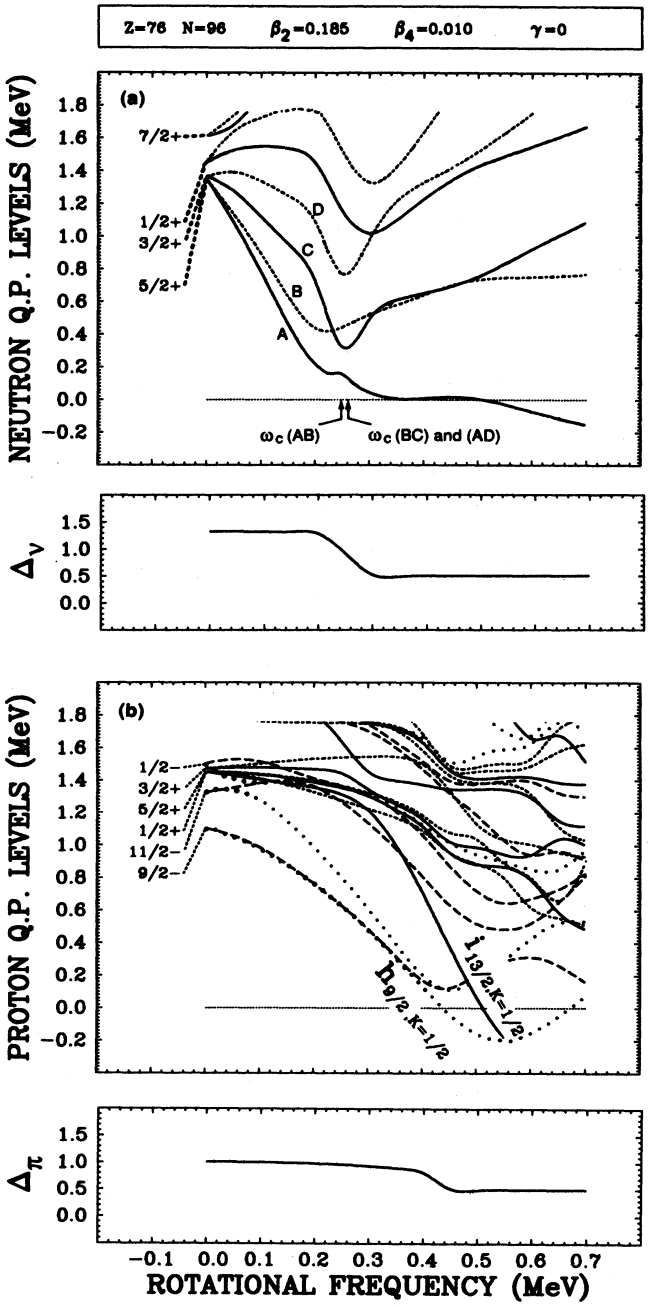

FIG. 17. (a) The quasiparticle orbitals in the rotating coordinate frame (Routhians) where the effects of pairing have been included for the neutrons at $N=96$. This figure is complementary to Fig. 16(a) which shows the corresponding spectra without pairing. For simplification, only the lowest positive parity levels are shown here. The bottom frame shows the properties of the pairing gap Δ calculated using the HFBC theory, but without particle number projection. (b) Similar to that in (a), but for the protons. In contrast to (a), all the quasiparticle levels are illustrated here. Note that the highly alignable negative-parity orbital has the structure of the one labeled $K^\pi=\frac{1}{2}^-$ rather than $\frac{9}{2}^-$. This is because of the sequence of two level crossings (see dotted curves showing crossings at $\omega_{cr1} \simeq 0.05$ MeV and $\omega_{cr2} \simeq 0.4$ MeV).

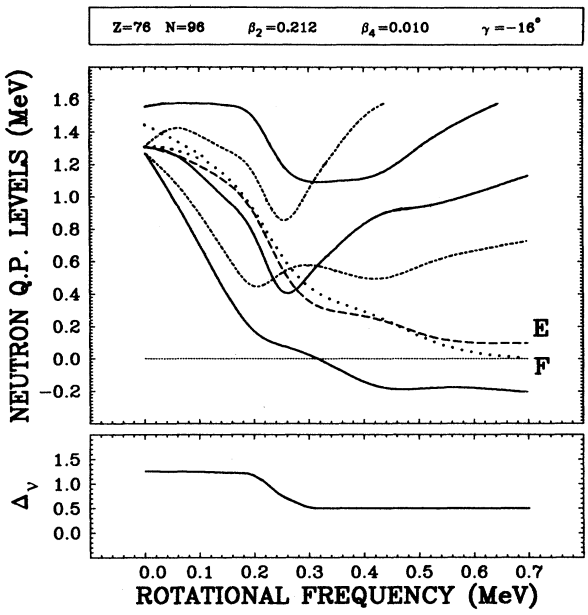

FIG. 18. Similar to Fig. 17(a) but for the negative-parity bands observed in this experiment and at the deformation corresponding to the low-spin part of the yrast spectrum ($\beta_2=0.21$). The low-lying negative-parity quasiparticle orbitals are labeled as E and F.

interpretation.

To give a more quantitative illustration of the effects of pairing, we show in Fig. 19 the sensitivity of the mechanism of alignment for the two variants of the calculation involving the neutron contributions to the alignment in ^{172}Os; *viz.*, the one with the pairing treated self-consistently and the other with Δ fixed at its $\omega=0$ value.

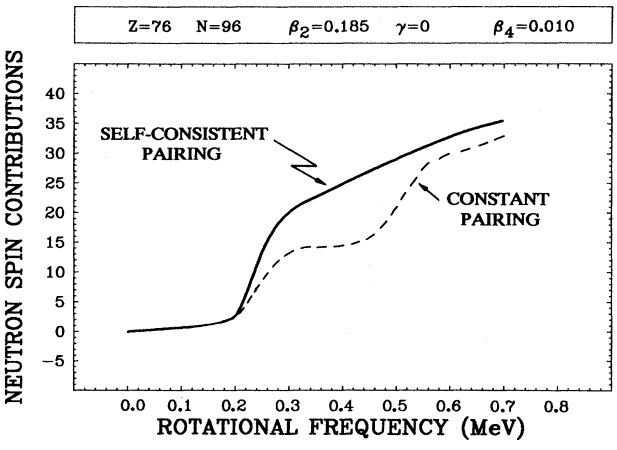

FIG. 19. Comparison between the calculated aligned angular momentum from the $i_{13/2}$ neutrons in ^{172}Os based on the self-consistent solutions (which implies a decrease of the pairing correlations as illustrated in Fig. 17) and that based on an artificially imposed constant pairing ansatz. The results indicate that a few units of $\hbar$ in the aligned angular momentum should be attributed to "quenched" pairing, showing the importance of treating the pairing self-consistently in the calculations.

The results are shown as a plot of I_x vs $\hbar\omega$. Not only are the numerical values of I_x markedly lowered in the case of imposed pairing constancy (such a constancy exaggerates the importance of pairing, especially at high rotational frequencies), but also the character of its dependence on ω is importantly changed in that the consecutive alignment and crossing frequencies are shifted.

VII. DISCUSSION

An inspection of the Fig. 17(a) positive-parity quasineutron Routhians, which are the active aligning orbitals at low spin in this mass region, reveals a rather complicated behavior in the frequency range $\hbar\omega=0.2-0.3$ MeV. These alignments originating from the levels labeled $K=\frac{5}{2}$, $\frac{3}{2}$, and $\frac{1}{2}$ are clearly strongly disturbed by mutually repulsive interactions. The first important two-quasiparticle excitations coupling to $(\pi,\alpha)=(+,0)$ are the AB, BC, and AD crossings (see Table III for notation). In Fig. 17(a) it can be seen that all of these crossings occur within a narrow frequency range ($\simeq 0.04$ MeV).

Because of the strong mixing expected between these configurations, it may be somewhat difficult to give a unique interpretation to each of the nearly degenerate crossing frequencies. However, we feel that it is possible to understand this complex situation for the $(+,0)$ configurations in ^{172}Os by using the simple standard band-crossing picture. We believe that the explanation proposed below contains the essence required in understanding the two anomalies at low frequencies observed in the ^{172}Os moment of inertia.

In this mass region, the first crossing of the ground-state rotational band is by the most alignable pair of $i_{13/2}$ neutrons, usually denoted as the s or AB band. In most cases, it has not been possible to observe the continuation of the ground band through this first crossing. In a few cases, however, this continuation has been followed (e.g., see Refs. 19–23). In these it was found that another crossing occurs soon after the first AB crossing and this was attributed to the BC and AD alignments. In ^{172}Os, we have also observed the continuation of the ground band through the first crossing (AB) region (labeled band 1 in Fig. 1). In Fig. 12(a), the high-alignment gain seen in these states indicates that the BC (or BC and AD) alignments probably have already taken place and at a very similar frequency to the band crossings in the yrast sequence. In the negative-parity sidebands the BC crossing is seen at $\hbar\omega\simeq 0.28$ MeV. It is interesting that the ground-BC (or $BCAD$) configuration changes occur at slightly lower frequency than the corresponding BC alignments in the negative-parity bands (e.g., $AE\rightarrow AEBC$). This same situation was seen for ^{158}Er by Simpson *et al.*[21] and by Riley (as referred to in Ref. 24), where the frequency difference is $\hbar\omega=0.03$ MeV.

Therefore, based on both the theoretical calculations and the experimental evidence, we must conclude that the first, second, and third quasineutron alignments in ^{172}Os all occur very close together. Furthermore, the observed gradual gain in alignment with frequency of the negative-parity bands implies that the BC alignment has

an associated interaction strength which is large. As seen in Fig. 13, this is true also in ^{173}Os where we observe a gradual gain in alignment through the frequency range of $\hbar\omega = 0.24-0.34$ MeV. This behavior, as in ^{172}Os, is attributed to the *BC* alignment. This large interaction strength is particularly important, since it means that the "effective" band interaction region is spread over a wider frequency range. In Fig. 11(a) of Ref. 20, where the alignment plot of ^{156}Dy below the *AB* crossing is shown, it is seen that the curvature for the ground band and its continuation is quite smooth and similar to ^{172}Os. Riley *et al.*[20] attributed this behavior to the strong interaction with the ground band from the *BC*(*AD*) crossing. Also note that in the Dy, Er, and Yb cases mentioned above, the *BC* interaction strength observed in the negative parity sidebands is of similar strength to that observed in the ground-band continuation. It is quite interesting that Bengtsson[25] has just reported the results of his HFBC calculations for ^{180}Pt and reaches a somewhat similar conclusion for a possible interpretation of the behavior in the low-frequency band-crossing region for this nucleus. That is, he finds it possible to interpret the behavior in the ^{180}Pt yrast sequence as arising from neutrons only, with the four-quasiparticle configuration *ABCD* playing a significant role in the properties seen in the experimental data.[26]

Another way to view this strong mixing region in ^{172}Os at $\hbar\omega = 0.2-0.3$ MeV is presented in Fig. 20. Here we have plotted the excitation energy E vs $I(I+1)$ for the ground band, for the *s* (or *AB*) band and for the continuation of the ground band. Straight-line extrapolations are drawn through data points outside the strong-mixing region. Their close-lying intersections with the ground band are consistent with our arguments above for multiple band crossings over a narrow frequency range. Note that the extrapolation of the so-called continuation of the ground band [which we term the *BC*(*AD*) band] comes from very close and, in fact, crosses the *s* (*AB*) band at lower spin. This does not happen in the Dy, Er, and Yb cases.

This coming together of excited (+,0) quasiparticle bands at low spin and the observation of a strong interaction strength of the *BC* alignment leads us to the following proposal for the explanation of the two low-spin anomalies in ^{172}Os. The first (*AB*), second (*BC*), and third (*AD*) band crossings occur at very similar frequencies ($\hbar\omega = 0.26-0.28$ MeV). However, because the interaction strength of the *BC* crossings is strong, the frequency range for the ground-*BC*(*AD*) crossing is smeared out sufficiently so as to perturb the ground band slightly below the *AB*-crossing region. This would explain the first anomaly in the yrast sequence at about spin 8 and $\hbar\omega = 0.24$ MeV. The second anomaly at $\hbar\omega = 0.27$ MeV is proposed to be the standard crossing by the *s* (*AB*) band.

Additional support for the above-proposed band-crossing picture is seen in Fig. 21, where the systematic tendencies in the evolution of the *AB*- and *BC*- band-crossing frequencies as a function of neutron number for Hf, W, and Os nuclei are presented (the data for this were taken from Refs. 1–3, 12, 13, 27–36). This comparison

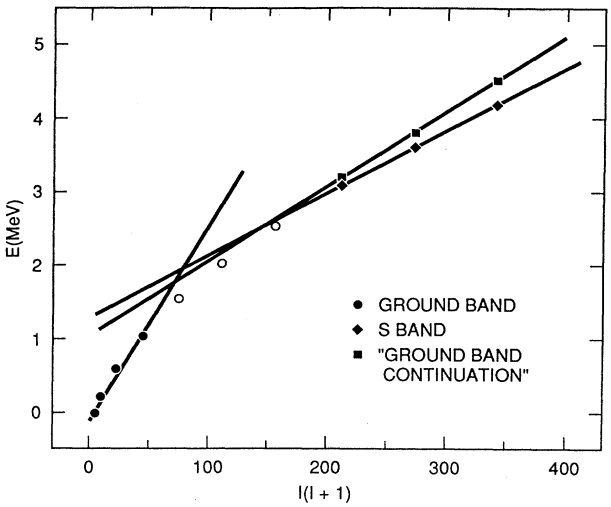

FIG. 20. The energies of states in the three positive-parity bands of ^{172}Os seen in the present experiment (the ground-state band, the *s* band, and the continuation of the ground-state band) are shown as a function of $I(I+1)$. The straight lines indicate the possible intersections between the three bands if they were noninteracting.

shows that the *BC* crossing frequency (in the negative-parity bands) decreases markedly while the *AB* crossing frequency (in the ground bands) increases as the neutron number approaches $N = 98$. This merging of crossing frequencies is also correlated with an increase in interaction strength for the *BC* crossing. Therefore, one would expect that the unique extraction of quasiparticle alignments, particularly in the (+,0) sequences, becomes very difficult when several orbitals are aligning over a narrow frequency range. Results for the Os isotopes on either side of ^{172}Os support these proposals above. The fact that in ^{170}Os the *BC* crossing is higher in frequency (see Ref. 3) and has a smaller interaction strength is consistent with the lack of a secondary anomaly in the yrast structure of that nucleus at low spin. However, in ^{174}Os we would expect a more complicated pattern, similar to ^{172}Os, but with the band crossings more smeared out. This is consistent with the experimental spectrum, where the yrast band is observed[1] to have a gain in alignment over a very wide frequency range, $\hbar\omega = 0.2-0.4$ MeV. Contrary to the conclusions of Durell *et al.*[1] that there are no band-crossing anomalies present in the ^{174}Os yrast-band data, it can be shown in a plot of the second moment of inertia for this nucleus that there are, indeed, two anomalies present.

In Fig. 22(a) we show an interesting comparison of the theoretical and experimental total aligned angular momentum along the yrast sequence of ^{172}Os where the particle-number projection variant[19] of the HFBC approach has been used in the calculations. While the backbending region is never described well by the cranking method, outside this range the agreement appears very good. Even the relatively detailed structures in the experimental curve find their analogs in theory as is shown in this figure. Note that this good agreement between experiment and theory is achieved only when the

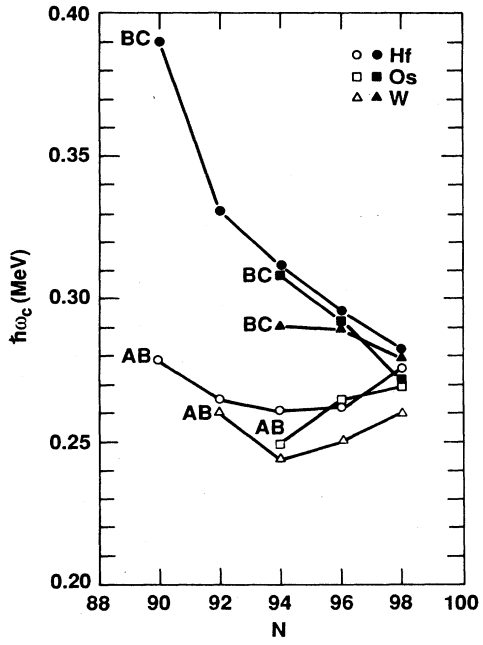

FIG. 21. Systematics of the experimental AB and BC band-crossing frequencies shown as a function of the neutron number N for the Hf, W, and Os nuclei (the data for this figure are from Refs. 1–3, 12, 13, 27–36). Note a characteristic tendency of ω_{AB} approaching ω_{BC} at $N\sim 98$. This pattern of crossings lends support to the calculated neutron quasiparticle diagrams in Figs. 17(a) and 18.

full microscopic calculation, including pairing and particle-number projection, is utilized. In this respect, it is significant to recognize that the decrease in the neutron pairing gap in Fig. 17(a) occurs at a lower frequency than is found in most cases, and that the frequency region of this decrease is just that at which the unusually low BC and AD band crossings take place.

We have already shown, in Fig. 19, the importance of including the quenching of the pairing correlations, an effect automatically accounted for in the self-consistent approach used here. We also stress the importance of using the evolving deformation parameters as a function of the frequency [as was done in the full calculation of Fig. 22(a)], as opposed to an artificially imposed constant deformation. This is illustrated in Fig. 22(b), where the calculation employed was the same as that used in Fig. 22(a) except for constant deformation. It is seen that the change in deformation, as suggested by the total-energy-surface calculations, does indeed yield improved agreement between experiment and theory.

Finally, we summarize a few of the conclusions to be drawn from the present work: (1) The nuclei considered possess rather "unusual" alignment properties resulting from their characteristic structure in terms of excited quasiparticles. This structure is dominated by strong interactions in the neutron quasiparticle crossings (AB, BC, and AD) and by the fact that they appear very close in terms of rotational frequencies. The first "anomaly" in the yrast line has been interpreted in terms of these nearly degenerate crossings. (2) The proton-induced alignment could not be identified in the present study. Theoretical arguments have been given to indicate its possible onset at $\hbar\omega\simeq 0.45$ MeV. (3) Calculations suggest a strong reduction in the neutron pairing gap over the frequency range $\hbar\omega=0.22$–0.28 MeV. It is deemed significant that this reduction in the neutron pairing gap

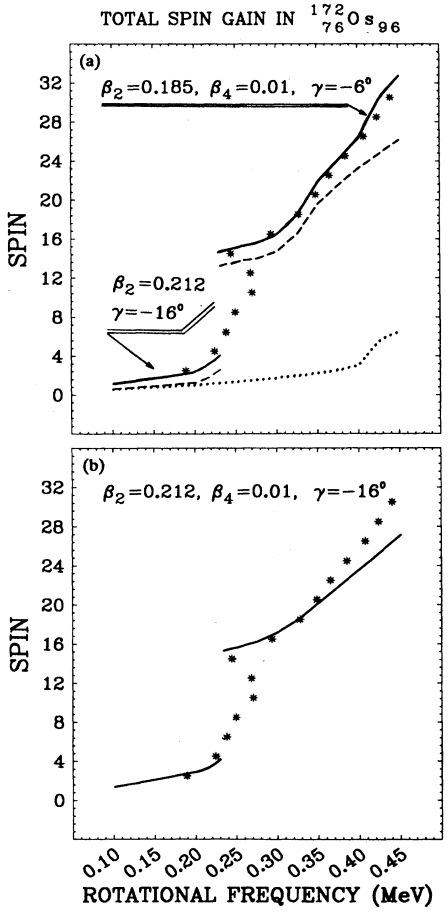

FIG. 22. (a) Comparison between the measured (asterisks) and calculated (solid line) spin versus rotational frequency. Dashed lines show contributions from the neutrons and the dotted lines show the contributions from the protons. The low- and high-spin portions of the theoretical line correspond to the deformations calculated for the corresponding frequency ranges [see Fig. 14(a) and discussion in the text]. Note that the structures in the experimental I vs ω sequence are reproduced quantitatively by using a five percent adjustment in the neutron pairing gap ($G=1.05$) and a one percent adjustment in the proton pairing gap ($G=1.01$). The backbending region cannot be described by the cranking model and, therefore, the theoretical lines are interrupted in this region. (b) Comparison between the measured (asterisks) and calculated (solid line) spin versus rotational frequency as in (a), except here the deformation was artificially held constant. This clearly illustrates that accounting for the changes in deformation, as suggested by the total-energy-surface calculations, provides improved agreement between experiment and theory.

occurs in the same region as does the unusually low *BC* band crossing.

ACKNOWLEDGMENTS

The authors would like to acknowledge the excellent support from the Holifield Heavy Ion Research Facility (HHIRF) accelerator staff and the indispensable help of Mark Whitley in maintaining the Compton-Suppression Spectrometer System. We also wish to thank Jerry Garrett for his helpful suggestions on the manuscript. This work was supported by the U.S. Department of Energy under Contract No. DE-AC05-84OR21400 with Martin Marietta Energy Systems, Inc.

---

*Present address: Oliver Lodge Laboratory, University of Liverpool, Liverpool L69 3BX, United Kingdom.
†Present address: University of Jyväskylä, Jyväskylä, Finland.

[1]J. L. Durell, G. D. Dracoulis, C. Fahlander, and A. P. Byrne, Phys. Lett. **115B**, 367(1982); Australian University Annual Report No. ANU-p/284, 1981, p. 25.
[2]J. C. Wells, N. R. Johnson, C. Baktash, I. Y. Lee, F. K. McGowan, M. N. Rao, L. L. Riedinger, V. Janzen, W. C. Ma, Shuxian Wen, Ze-Min Chen, P. B. Semmes, G. A. Leander, and Y. S. Chen, Phys. Rev. C **36**, 431 (1987).
[3]G. D. Dracoulis, R. A. Bark, A. E. Stuchbery, A. P. Byrne, A. M. Baxter, and F. Riess, Nucl. Phys. **A486**, 414 (1988).
[4]J. D. Garrett and S. Frauendorf, Phys. Lett. **108B**, 77 (1982).
[5]S. T. Hsieh, M. M. King Yen, and T. T. S. Kuo, J. Phys. G **14**, L31 (1988).
[6]A. Virtanen, N. R. Johnson, C. Baktash, I. Y. Lee, F. K. McGowan, M. A. Riley, J. C. Wells, and J. Dudek, Bull. Am. Phys. Soc. **33**, 1585 (1988).
[7]A. Virtanen, N. R. Johnson, F. K. McGowan, M. A. Riley, I. Y. Lee, C. Baktash, J. Dudek, and J. C. Wells, Oak Ridge National Laboratory Report No. ORNL-6508, 1988, p. 65.
[8]A. Virtanen, M. A. Riley, N. R. Johnson, F. K. McGowan, I. Y. Lee, C. Baktash, J. Dudek, J. Y. Zhang, F. Dönau, and J. C. Wells (unpublished).
[9]K. S. Krane, R. M. Steffen and R. M. Wheeler, Nuclear Data Tables **11**, 351 (1973).
[10]Julian program PACE (unpublished).
[11]W. Walus, N. Roy, S. Jónsson, L. Carlen, H. Ryde, G. B. Hagemann, B. Herskind, J. D. Garrett, Y. S. Chen, J. Almberger, and G. Leander, Physica **24**, 324 (1981).
[12]R. Chapman, J. C. Lisle, J. N. Mo, E. Paul, A. Simcock, J. C. Willmott, J. R. Leslie, H. G. Price, P. M. Walker, J. C. Bacelar, J. D. Garrett, G. B. Hagemann, B. Herskind, A. Holm and P. J. Nolan, Phys. Rev. Lett. **51**, 2265 (1983).
[13]J. Recht, Y. K. Agarwal, K. P. Blume, M. Guttormsen, H. Hübel, H. Kluge, K. H. Maier, A. Maj, N. Roy, D. J. Decman, J. Dudek, and W. Nazarewicz, Nucl. Phys. **A440**, 366 (1985).
[14]S. Cwiok, J. Dudek, W. Nazarewicz, J. Skalski, and T. Werner, Comput. Phys. Commun. **46**, 379 (1987).
[15]M. de Voigt, J. Dudek, and Z. Szymanski, Rev. Mod. Phys. **55**, 949 (1983).
[16]J. Dudek, Proceedings of the Winter Meeting on Nuclear Physics, Bormio, 1987, edited by I. Iori (unpublished).
[17]P. Ring and P. Schuck, *The Nuclear Many Body Problem*, (Springer, New York, 1980).
[18]P. Møller and J. R. Nix, Nucl. Phys. **A361**, 117 (1981); At. Data Nucl. Data Tables **26**, 165 (1981).
[19]J. Dudek, T. Werner and L. L. Riedinger, Phys. Lett. B **211**, 252 (1988).
[20]M. A. Riley, J. Simpson, J. F. Sharpey-Schafer, J. R. Cresswell, H. W. Cranmer-Gordon, P. D. Forsyth, D. Howe, A. H. Nelson, P. J. Nolan, P. J. Smith, N. J. Ward, J. C. Lisle, E. Paul, and P. M. Walker, Nucl. Phys. **A486**, 456 (1988).
[21]J. Simpson, P. A. Butler, P. D. Forsyth, J. F. Sharpey-Schafer, J. D. Garrett, G. B. Hagemann, B. Herskind, and L. P. Ekström, J. Phys. G **10**, 383 (1984).
[22]J. Simpson, M. A. Riley, J. R. Cresswell, D. V. Elenkov, P. D. Forsyth, G. B. Hageman, D. Howe, B. M. Nyakó, S. Ogaza, J. C. Lisle, and J. F. Sharpey-Schafer, J. Phys. G **13**, 847 (1987).
[23]S. Jónsson, N. Roy, H. Ryde, W. Walus, J. Kownacki, J. D. Garrett, G. B. Hagemann, B. Herskind, R. Bengtsson, and S. Åberg, Nucl. Phys. **A449**, 537 (1986).
[24]J. D. Garrett, Nucl. Phys. **A421**, 313c (1984).
[25]R. Bengtsson, in *Proceedings of the International Conference on Contemporary Topics Nuclear Structure Physics, Cocoyoc, Mexico, 1988,* edited by R. F. Casten, A. Frank, M. Moshinsky, and S. Pittel (World Scientific, Singapore), p. 317.
[26]M. J. A. deVoigt (private communication).
[27]C. R. Bingham, L. L. Riedinger, L. H. Courtney, Z. M. Liu, A. J. Larabee, M. Craycraft, D. J. G. Love, P. J. Nolan, A. Kirwan, D. Thornley, P. Bishop, A. H. Nelson, M. A. Riley, and J. C. Waddington, J. Phys. G **14**, L77 (1988).
[28]J. N. Mo, S. Sergiwa, R. Chapman, J. C. Lisle, E. Paul, J. C. Willmott, J. Hattula, M. Jääskeläinen, J. Simpson, P. M. Walker, J. D. Garrett, G. B. Hagemann, B. Herskind, M. A. Riley, and G. Sletten, Nucl. Phys. **A472**, 295 (1987).
[29]K. P. Blume, H. Hübel, M. Murzel, J. Recht, K. Theine, H. Kluge, A. Kuhnert, K. H. Maier, A. Maj, M. Guttormsen, and A. P. deLima, Nucl. Phys. **A464**, 445 (1987).
[30]E. M. Beck, M. A. Deleplanque, R. M. Diamond, R. J. McDonald, F. S. Stephens, J. C. Bacelar, and J. E. Draper, Z. Phys. A **327**, 397 (1987).
[31]J. C. Lisle, J. D. Garrett, G. B. Hagemann, B. Herskind, and S. Ogaza, Nucl. Phys. **A366**, 281 (1981).
[32]C. Baktash, M. L. Halbert, D. C. Hensley, N. R. Johnson, I. Y. Lee, J. W. McConnell, F. K. McGowan, C. M. Steele, M. Carpenter, V. P. Janzen, and L. L. Riedinger, Bull. Am. Phys. Soc. **33**, 1585 (1988); Oak Ridge National Laboratory Report No. ORNL-6508, 1988, p. 72.
[33]J. Gerl, G. D. Dracoulis, A. P. Byrne, A. R. Poletti, S. J. Poletti, and A. E. Stuchbery, Nucl. Phys. **A443**, 348 (1985).
[34]G. D. Dracoulis, H. Hübel, A. P. Byrne, R. F. Davie, Nucl. Phys. **A405**, 363 (1983).
[35]G. D. Dracoulis, P. M. Walker, and A. Johnston, J. Phys. G **4**, 713 (1978).
[36]J. C. Lisle and J. D. Garrett (private communication).

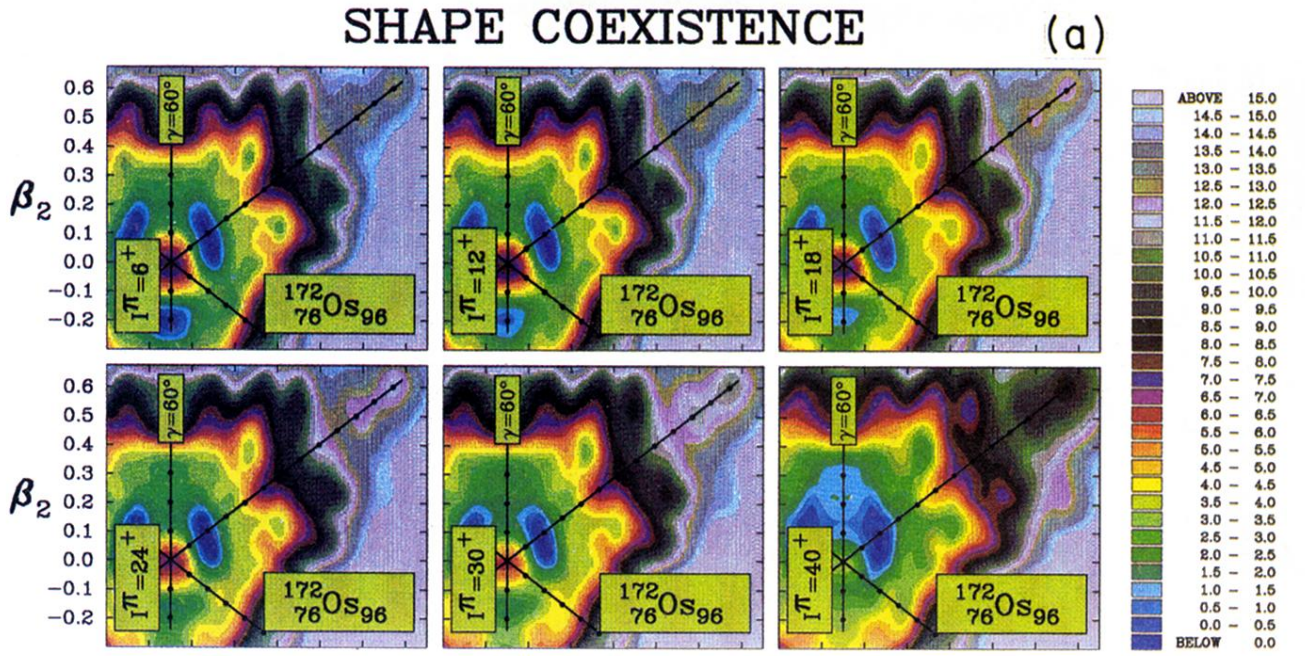

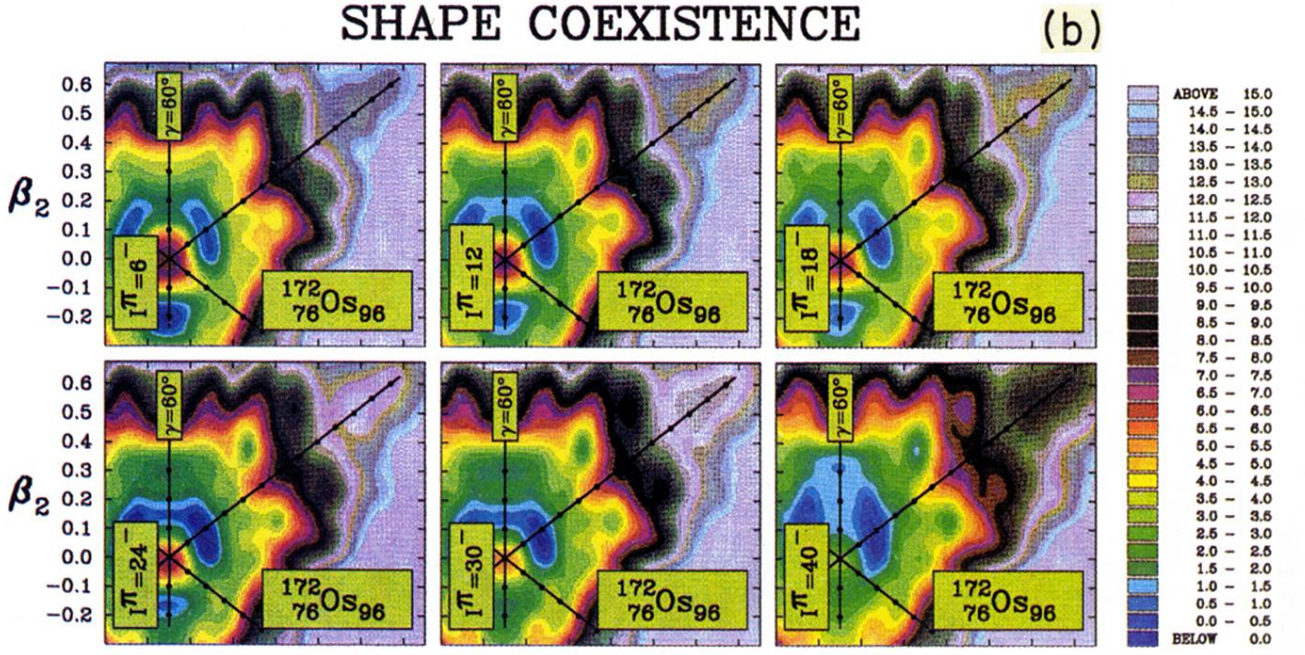

FIG. 14. (a) Total-energy surfaces for positive-parity configurations of ^{172}Os calculated with the extended Strutinsky method (see text). The spin-parity values are given explicitly. The coordinate system is that of the standard (β,γ)-plane with the following convention: vertical axis ($\gamma=60°$) corresponds to increasing oblate shape deformations with the symmetry axis parellel to the cranking axis (noncollective rotation); the $\gamma=0°$ axis (near diagonal) corresponds to increasing elongation where the symmetry axis is perpendicular to the rotation axis (collective rotation); the $\gamma=-60°$ corresponds to the family of oblate shapes identical to those on the $\gamma=+60°$ axis, except that now the symmetry axis is again perpendicular to the rotation axis; finally, the $\gamma=-120°$ axis corresponds to noncollective rotation of the prolate nucleus with the symmetry axis parallel to the spin axis. (b) Similar to that in (a), but for a number of negative-parity configurations.